

# Simultaneous removal of Cu (II) and Cr (VI) ions from petroleum refinery wastewater using ZnO/Fe<sub>3</sub>O<sub>4</sub> nanocomposite

E. Y. Shaba, J. O. Tijani, J. O. Jacob & M. A. T. Suleiman

To cite this article: E. Y. Shaba, J. O. Tijani, J. O. Jacob & M. A. T. Suleiman (2022) Simultaneous removal of Cu (II) and Cr (VI) ions from petroleum refinery wastewater using ZnO/Fe<sub>3</sub>O<sub>4</sub> nanocomposite, Journal of Environmental Science and Health, Part A, 57:13-14, 1146-1167, DOI: [10.1080/10934529.2022.2162794](https://doi.org/10.1080/10934529.2022.2162794)

To link to this article: <https://doi.org/10.1080/10934529.2022.2162794>



Published online: 05 Jan 2023.



Submit your article to this journal [↗](#)



Article views: 32




View related articles [↗](#)



View Crossmark data [↗](#)



## Simultaneous removal of Cu (II) and Cr (VI) ions from petroleum refinery wastewater using ZnO/Fe<sub>3</sub>O<sub>4</sub> nanocomposite

E. Y. Shaba , J. O. Tijani, J. O. Jacob and M. A. T. Suleiman

Department of Chemistry, Federal University of Technology, Minna, Niger, Nigeria

### ABSTRACT

The presence and removal of heavy metals such as Cu(II) as well as Cr(VI) in petroleum refinery wastewater calls for concerted efforts due to their mobility, toxicity, bioaccumulation, and non-biodegradability in the environment. In this present work, zinc oxide (ZnO), iron oxide (Fe<sub>3</sub>O<sub>4</sub>) nanoparticles and ZnO/Fe<sub>3</sub>O<sub>4</sub> nanocomposites were synthesized via simple sol-gel and chemical reduction methods; characterized using different analytical tools and then applied as nanoadsorbent to sequester Cu(II) and Cr(VI) ions from Petroleum Refinery wastewater via batch adsorption process. Cu(II) and Cr(VI) adsorption processes were examined with respect to contact time (kinetic effect), nanoadsorbent dosage, isotherm equilibrium, and thermodynamic parameters. ZnO/Fe<sub>3</sub>O<sub>4</sub> nanocomposites with higher surface area (39.450 m<sup>2</sup>/g) have a mixture of rod-like and spherical shapes as compared to ZnO and Fe<sub>3</sub>O<sub>4</sub> nanoparticles with spherical shape only and surface areas of 8.62 m<sup>2</sup>/g and 7.86 m<sup>2</sup>/g according to the high-resolution scanning electron microscopy (HRSEM) and Brunauer–Emmett–Teller (BET) analysis. The X-ray diffractometer (XRD) results revealed the formation of hexagonal wurtzite structure of ZnO and the face-centered cubic structure phase of Fe<sub>3</sub>O<sub>4</sub> nanoparticles, after the formation of the ZnO/Fe<sub>3</sub>O<sub>4</sub> nanocomposites the phases of the nanoparticles were not affected but the diffraction peaks shifted to higher 2θ degree. The average crystallite size of ZnO and Fe<sub>3</sub>O<sub>4</sub> nanoparticles and ZnO/Fe<sub>3</sub>O<sub>4</sub> nanocomposites were 20.12, 26.36 and 14.50 nm respectively. The maximum removal efficiency of Cu (II) (92.99%) and Cr (VI) (77.60%) by ZnO/Fe<sub>3</sub>O<sub>4</sub> nanocomposites was higher than 85.83%; 65.19% for Cu (II) and 80.57%; 62.53 for Cr (VI) using ZnO and Fe<sub>3</sub>O<sub>4</sub> nanoadsorbents individually under the following conditions: contact time (15), dosage (0.08 g) and temperature (30 °C). The experimental data for Cu (II) and Cr (VI) ion removal fitted well to the pseudo-second-order kinetic and Langmuir isotherm models. The thermodynamic study suggested that the removal of the two metal ions from petroleum wastewater was endothermic. The reusability study after the fourth adsorption-desorption cycle indicated the stability of ZnO/Fe<sub>3</sub>O<sub>4</sub> nanocomposites with 85.51% and 69.42% removal efficiency of Cu (II) and Cr (VI). The results showed that ZnO/Fe<sub>3</sub>O<sub>4</sub> nanocomposite achieves higher performance than ZnO and Fe<sub>3</sub>O<sub>4</sub> alone in the removal of Cu (II) and Cr (VI) ions from the petroleum refinery wastewater.

**ABBREVIATIONS:** 1/n: the intensity adsorption; B (J/mol): the Temkin constant; β: the extent of surface coverage (g/mg); Ce: Final concentration of the metal ions after the interaction with the adsorbent (mg/L); Co: Initial concentration of the metal ions after the interaction with the adsorbent (mg/L); D: crystallite size; EDS: Energy Dispersive Spectroscopy; ε: Polanyi potential; HRSEM: High-Resolution Scanning Electron Microscopy; K1: is a pseudo-first-order rate constant (min<sup>-1</sup>); K2: is pseudo-second order the rate constant (min<sup>-1</sup>); Kd: is the adsorbate distribution coefficient; kD-R: is the adsorption energy constant; KL: Langmuir constant; KF: Freundlich adsorption capacity; KT: Equilibrium binding constant (L/g); k: 0.9 is a constant; m(g): is the mass of the ZnO, Fe<sub>3</sub>O<sub>4</sub> and the ZnO/Fe<sub>3</sub>O<sub>4</sub> nanocomposites (g); qmax: Maximum adsorption capacity (mg/g); qe: Amounts of heavy metals at time t (min); qt: the amounts of heavy metals at equilibrium (mg/g); R: Universal gas constant; T: Absolute solution temperature (K); V: Volume of the petroleum wastewater (mL); X-ray: diffraction (XRD); ΔS°: Standard entropy change (J/mol.K); ΔH°: Standard enthalpy change (kJ/mol); ΔG°: Gibbs free energy (kJ/mol); β: Full width at half maximum (FWHM); α: Adsorption rate (mg/g min); θ: Angle of Bragg; λ: Wavelength (1.54 Å)

### ARTICLE HISTORY

Received 6 October 2022  
Accepted 12 December 2022

### KEYWORDS

ZnO/Fe<sub>3</sub>O<sub>4</sub> nanocomposite; sol-gel; heavy metal; adsorption; regeneration; kinetic and isotherm model

### Introductions

Water is essential for healthy ecosystems, socioeconomic development, food and energy production as well as human growth.<sup>[1]</sup> However, the problem of water scarcity has emerged as a major obstacle to human development due to rapid industrial and urban expansion.<sup>[2]</sup> It has been reported

that by 2025 developing countries will be most affected by water pollution, and half of humanity will reside in water-scarce regions.<sup>[3]</sup> The pollution of water bodies through the exploration and refining of crude oil results in the production of petroleum-related products such as wastewater.<sup>[4]</sup> The wastewater generated by the petroleum refinery

industries contains highly mobile, non-biodegradable pollutants such as heavy metals.<sup>[5]</sup> Heavy metals include cadmium, nickel, copper, zinc, chromium, and manganese amongst others. The presence of copper and chromium in petroleum refinery wastewater has been linked to the nature of crude oil rock<sup>[6]</sup> and the drilling fluids used during crude oil extraction.<sup>[7]</sup>

Heavy metals are highly non-biodegradable persistent, and mobile in aqueous media and accumulate in living organisms causing threats to the environment because of their toxicity, for instance, exposure to Cu(II) has been associated with renal dysfunction, anemia, niacin deficiency damage to the liver, brain, kidney, leukemia, tumor, learning disabilities, chronic fatigue, vomiting, headache, high blood pressure, behavioral disorders, muscle, joint and abdominal pains.<sup>[8,9]</sup> Inhalation of Cr (VI) ions has been linked to nasal ulcers, nasal irritation, lung and skin ulcers.<sup>[10]</sup> According to studies, Cr (III) results in reactive intermediates that increase genotoxicity, cytotoxicity and carcinogenicity, as well as oxidative tissue destruction and oxidative stress.<sup>[11]</sup>

Various methods such as biological,<sup>[12]</sup> flocculation,<sup>[13]</sup> precipitation,<sup>[14]</sup> co-precipitation,<sup>[15]</sup> electrolysis,<sup>[16]</sup> and membrane,<sup>[17]</sup> ion exchange,<sup>[18]</sup> coagulation<sup>[19]</sup> have been used for the treatment of wastewater. However, these methods are time-consuming, costly, not environmentally friendly and inefficient for the complete removal of these pollutants.<sup>[14]</sup> Thus, there is a need for an alternative method that can effectively remove the pollutants in petroleum refinery wastewater even at low concentration. Adsorption technology is considered more effective and economical for removing heavy metals from industrial wastewater than other conventional wastewater treatment technologies.<sup>[20]</sup> Different adsorbents such as zeolites, agricultural wastes, clay and activated carbon have been used by many scientists to remove heavy metals<sup>[20]</sup>. Despite their effectiveness in removing heavy metals, these adsorbents have some drawbacks. For example, the use of adsorbents from carbon sources for the treatment of petroleum refinery wastewater has been linked to the generation of dimethyl disulfide ( $C_2H_6S_2$ ) as a byproduct and competition with other organic compounds during the adsorption process.<sup>[20]</sup> The disadvantages of zeolites and clay include poor stability and regeneration over a wide range of pH.<sup>[21]</sup>

The use of metal oxides and their composites as nano-adsorbent have been globally recognized as an efficient material for heavy metals removal due to their high adsorption capacity, enhanced functionality and large surface area, stability over a wide range of pH, and their small crystallite size.<sup>[22]</sup> Zinc oxide (ZnO) in particular has received a lot of attention among researchers because of its chemical and physical stability, environmental friendliness, mild operating conditions, specific surface area and regular pore structure.<sup>[23]</sup> Other interesting characteristics of ZnO nanoparticles include non-toxicity, biocompatibility, and cost-effectiveness. ZnO nano-adsorbent has been used to remove heavy metals in the aqueous matrix. For instance,<sup>[24]</sup> employed spherical ZnO nanoparticles to remove 96% of Cr (VI) ions at 210 min, pH of 2.5, temperature ( $60^\circ C$ ), and dose (0.5g). Using ZnO nanoparticles under the reaction conditions of pH of 4.8,

concentration (8 mg/L) and room temperature,<sup>[25]</sup> has also observed 98.4% removal of Cu (II) from an acidic solution.

Another metal oxide used to remove heavy metals is magnetite ( $Fe_3O_4$ ) nanoparticles due to their unique characteristics such as superparamagnetic, amphoteric nature, easy dispersibility in aqueous solution, large surface area, faster separation and, no generation of secondary pollutants.<sup>[26]</sup> Many researchers have studied the elimination of heavy metals using  $Fe_3O_4$  nanoparticles as an adsorbent. For instance,<sup>[27]</sup> reported 72% removal efficiency of Cr (VI) ions using  $Fe_3O_4$  nanoadsorbent at pH (3), temperature ( $30^\circ C$ ), adsorbent dosage (10 g) and contact time (110 min), concentration (10 m/L). Another researcher reported 88.83% removal efficiency of Cr (VI) ions and 96.10% of Cu (II) ions by  $Fe_3O_4$  nanoadsorbent under the following conditions: pH (4), temperature ( $25^\circ C$ ), adsorbent dosage (2.5 g), contact time (90 min), and concentration of 1 mg/L.<sup>[28]</sup>

The use of individual nanoparticles such as zinc oxides (ZnO) for the heavy metals removal from wastewater has been linked to some limitations which include aggregation and instability in an aqueous system and poor separation after the adsorption process.<sup>[29]</sup> Additionally, magnetite ( $Fe_3O_4$ ) nanoparticles are easily oxidized with oxygen and are corroded by acids and bases because of the presence of Fe (II) in their structures.<sup>[30]</sup> Due to some of these limitations, the development of a nanocomposite for heavy metal removal is essential. The performance of various nanocomposites on heavy metal ions removal from wastewater has been evaluated and reported. For instance,<sup>[5]</sup> Studied Cr (VI) ion removal from the aqueous phase by ZnO/guar gum composite and the authors reported maximum removal efficiency of 95.60%, at a contact time of 50 min, initial metal concentration (25 mg/L), nanoadsorbent dose of 1.0 g/L and pH of 7. Similarly,<sup>[31]</sup> studied Cu (II) removal using ZnO/hollow fiber composite and found that the nanoadsorbent removed 92% of Cu (II) ion under the following conditions of concentration of  $50\text{ mg L}^{-1}$ , contact time of 3 h and pH of 8. Another research by<sup>[32]</sup> showed that the  $Fe_3O_4$ /activated carbon nanocomposites have the potential of removing 99.21% from aqueous solution under the following conditions: concentration (12 mg/L), 40 min of contact time and 0.5 g/L nanoadsorbent dosage.

The reusability of spent nanoadsorbent is of primary economic significance, first to minimize operating costs and, second, to tackle challenges associated with spent nanoadsorbent disposal, which is a costly and resource-intensive option. Many researchers have used different eluents such as nitric acid ( $HNO_3$ ), hydrochloric (HCl), acetic acid ( $CH_3COOH$ ), sulfuric acid ( $H_2SO_4$ ), calcium chloride ( $CaCl_2$ ), potassium nitrate ( $KNO_3$ ), sodium hydroxides (NaOH), sodium chloride (NaCl), sodium nitrate ( $NaNO_3$ ), Ethylenediamine tetraacetic acid (EDTA) and water ( $H_2O$ ) as desorbing agent for the regeneration of heavy metals.<sup>[33]</sup> Among the aforementioned desorbing agents acids are the most effective and extensively utilized.

According to the literature, numerous studies have reported the use of nanoadsorbent to remove Cu (II) and Cr (VI) ions. However, there is currently a paucity of information in the literature on the use of and ZnO/ $Fe_3O_4$  nanocomposites for the sequestration of Cu (II) and Cr (VI) ions from real industrial wastewater. Much of the research

conducted on the use of nanoadsorbent for the treatment of Cu (II) and Cr (VI) did not study the adsorption-desorption of the nanoadsorbents, indicating that once the adsorbent has been used up, it must be disposed of which may result in an environmental issue. As a result, nanoadsorbent regeneration and reusability are critical to making the adsorption process cost-effective, environmentally friendly and reducing adsorbent requirements. In this research, The ZnO/Fe<sub>3</sub>O<sub>4</sub> nanocomposites were first synthesized through sol-gel methods and the produced nanocomposites were characterized by different analytical tools to determine their physicochemical properties. The adsorptive potentials of ZnO/Fe<sub>3</sub>O<sub>4</sub> nanocomposites as a nanoadsorbent for the adsorption of Cu (II) and Cr (VI) ions in petroleum refinery wastewater and their re-usability to ascertain the cost-effectiveness was evaluated. The adsorption isotherms, kinetics models, and thermodynamics for the adsorption of Cu (II) and Cr (VI) on ZnO/Fe<sub>3</sub>O<sub>4</sub> nanocomposites were also studied.

### Materials and methods

Analytical grade Iron (III) chloride tetrahydrate, sodium hydroxide (NaOH), zinc nitrate hexahydrate and polyvinyl pyrrolidone (PVP) (95%) were obtained from Sigma Aldrich. The petroleum refinery wastewater from Kaduna Refining and Petrochemical Company (KRPC).

### Synthesis of zinc oxide/iron oxide (ZnO/Fe<sub>3</sub>O<sub>4</sub>) nanocomposites

ZnO nanoparticles were synthesized by measuring 60 mL of 0.1 M zinc nitrate hexahydrate into a beaker (250 mL). This was followed by the slow addition of 25 mL of 1.0 M NaOH solution to the mixture. To the same mixture, 10 mL of Polyvinylpyrrolidone (5%) was added. The mixture was placed on a magnetic stirrer and stirred at 250 rpm. This was accompanied by the formation of a gel-like solution and was left overnight before being dried at 100 °C in an oven and then calcined at 450 °C for 2 h respectively. Secondly, Fe<sub>3</sub>O<sub>4</sub> was synthesized by measuring 25 mL of 0.1 M iron (III) chloride tetrahydrate into a 250 mL beaker and stirring for 15 min. Then 30 mL of 0.3 M sodium borohydride was added to the iron chloride solution and stirred continuously at 30 °C for 15 mins. 10 mL of the 5% PVP was added to the solution resulting in the formation of a brownish sol-gel-like mixture. The brownish gel-like mixture was later dried at 100 °C in the oven overnight. The dried samples were calcined at 200 °C for 2 h to give Fe<sub>3</sub>O<sub>4</sub> nanoparticles.<sup>[34]</sup> Moreover, the ZnO/Fe<sub>3</sub>O<sub>4</sub> nanocomposites were synthesized using the same sol-gel method, which involved measuring 0.1 M Iron (III) chloride tetrahydrate into a 250 mL beaker, the addition of 0.3 M sodium borohydride to the solution, stirring continuously at 30 °C for 15 minutes, and then adding 0.1 M zinc nitrate hexahydrate. The mixture was rapidly stirred for 2 hours, then aged for 4 h followed by calcination in the furnace at 450 °C for 2 h.<sup>[35]</sup>

### Characterization of ZnO, Fe<sub>3</sub>O<sub>4</sub>, nanoparticles and ZnO/Fe<sub>3</sub>O<sub>4</sub> nanocomposites

The phases and crystallite sizes of the produced ZnO, Fe<sub>3</sub>O<sub>4</sub>, nanoparticles, and ZnO/Fe<sub>3</sub>O<sub>4</sub> nanocomposites were determined using an advanced X-ray diffractometer (Bruker AXS D8) with Cu K radiation. The powdered samples were dispersed on a degreased glass slide and the scanning and diffraction pattern was obtained from 20° - 90°. The results obtained were compared to the diffraction peaks from the Joint Committee on Powder Diffraction Standard (JCPDS) and accessible d-spacing data was done. The morphologies of the ZnO, Fe<sub>3</sub>O<sub>4</sub>, nanoparticles, and ZnO/Fe<sub>3</sub>O<sub>4</sub> nanocomposites were analyzed using a Zeiss Auriga HRSEM, where 0.05 mg of each sample were sputter-coated with Au-Pd and then mounted on carbon adhesive tape. For imaging, the microscope was run at a high electron tension of 5 kV. Additionally, the elemental composition of the produced ZnO, Fe<sub>3</sub>O<sub>4</sub>, nanoparticles, and ZnO/Fe<sub>3</sub>O<sub>4</sub> nanocomposites were determined using energy dispersive spectroscopy (EDS) coupled high-resolution scanning electron microscopy (HRSEM) (EDS). The BET surface area and average pore volume distributions were determined from the plot of the volume adsorbed (cm<sup>3</sup>/g STP) against relative pressure. NovawinQuantachrome device (NOVA 2400e) with N<sub>2</sub> as an adsorbate on a micrometre ASAP 2020 was applied to determine the surface area, total pore volume, and pore size of the various nanomaterial. Before the analysis, degassing of the samples was done at 90 °C for 4 h under inert nitrogen gas flow, to get rid of adsorbed moisture and other compounds that may block the pores. The functional groups present in ZnO, Fe<sub>3</sub>O<sub>4</sub>, nanoparticles, and ZnO/Fe<sub>3</sub>O<sub>4</sub> nanocomposites were determined using Fourier transform infrared (FTIR) spectra (Thermo Scientific Nicolet iS5) at a wavenumber range between 4,000-500 cm<sup>-1</sup>.

### Batch adsorption

#### Effect of contact time

ZnO, Fe<sub>3</sub>O<sub>4</sub> and ZnO/Fe<sub>3</sub>O<sub>4</sub> nanoadsorbents were applied for the removal of Cu (II) and Cr (VI) ions from petroleum refinery wastewater. Different conical flasks were filled with 0.05 g ZnO, Fe<sub>3</sub>O<sub>4</sub>, and ZnO/Fe<sub>3</sub>O<sub>4</sub> nanocomposite after which 50 mL of refinery wastewater was measured. The mixture was agitated continuously at varied contact times of 1, 5, 10, 15, 20, and 25 minutes at 30 °C in the conical flasks. The liquid phase was separated from the reaction mixture after each contact period, and the concentrations of the remaining metal ions were then quantified via Atomic absorption spectroscopy (AAS).<sup>36</sup>

#### Effect of nanoadsorbent dosage

In separate conical flasks, the removal of Cu (II) and Cr (VI) ions from petroleum refinery wastewater was investigated at various nanoadsorbent doses (0.02, 0.04, 0.06, 0.08, 0.1 to 0.12 g/50 mL). The solution was agitated continuously on a magnetic stirrer at 250 rpm for 15 minutes. The liquid phase was separated from the reaction mixture after each contact period, and the concentrations of the remaining metal ions were then quantified by AAS.<sup>[36]</sup>



### Effect of temperature

In separate conical flasks, 50 mL of petroleum refinery wastewater was measured, and 0.05 g of the nanoadsorbent was added after which the mixture was swirled with a stirrer for 15 minutes. Cu (II) and Cr (VI) ions were removed from refinery wastewater at 30 °C, 40 °C, 50 °C, 60 °C, 70 °C, and 80 °C controlled by a heat regulator coupled to a shaker. The liquid phase was separated from the reaction mixture after each contact period, and the concentrations of the remaining metal ions were then quantified via AAS.<sup>[36]</sup>

### Leaching and desorption studies

Different concentrations (0.025, 0.08, and 0.1 mol dm<sup>-3</sup>) of nitric acid (HNO<sub>3</sub>) solutions were used in the desorption experiments. The nanocomposites that had previously been exposed to petroleum refinery wastewater were drained and mixed with 20 mL of HNO<sub>3</sub> solutions. The orbiter shaker was used to agitate the samples for 15 minutes. After desorption, the level of Cu (II) and Cr (VI) ions in the liquid phase was quantified by AAS. The desorption efficiency was calculated according to Eq. (1). The concentration of Zn (II) and Fe (II) ions in the leachate was also determined after the desorption process at different concentrations of acids using AAS.

Desorption efficiency(%)

$$= \frac{\text{Concentration of Cu (II) and Cr (VI) ions desorbed}}{\text{Concentration of Cu (II) and Cr (VI) ions adsorbed}} \times 100 \quad (1)$$

### Reusability

The exhausted nanoadsorbents were cycled four times to test the reusability of ZnO, Fe<sub>3</sub>O<sub>4</sub> nanoparticles, and ZnO/Fe<sub>3</sub>O<sub>4</sub> nanocomposites. 0.1 mol dm<sup>-3</sup> HNO<sub>3</sub> solutions were used as desorption agents. The ZnO, Fe<sub>3</sub>O<sub>4</sub> nanoparticles, and ZnO/Fe<sub>3</sub>O<sub>4</sub> nanocomposites that had previously been exposed to refinery wastewater were drained and mixed with 20 mL of HNO<sub>3</sub> solutions. The orbiter shaker was used to agitate the samples for 15 minutes. Desorbed ZnO, Fe<sub>3</sub>O<sub>4</sub> nanoparticles, and ZnO/Fe<sub>3</sub>O<sub>4</sub> nanocomposites were applied as a nanoadsorbent for the adsorption of Cu (II) and Cr (VI) ions. 0.05 g of desorbed ZnO, Fe<sub>3</sub>O<sub>4</sub> and ZnO/Fe<sub>3</sub>O<sub>4</sub> nanocomposites each were added to 50 mL of the petroleum wastewater in conical flasks. The mixture was stirred for 15 minutes at 30 °C and a pH of 6.25 on a magnetic stirrer. The liquid phase was separated from the reaction mixture after each contact period, and the concentrations of the remaining metal ions were then quantified via AAS.<sup>[37]</sup>

### Data analysis

The removal efficiency of the amount of Cu (II) and Cr (VI) ions by the nanoadsorbents were estimated as shown in Eq. (2).

$$q_e = \frac{(C_o - C_e) \times V}{m} \quad (1)$$

$$\% \text{ Removal} = \frac{C_o - C_e}{C_o} \times 100 \quad (2)$$

### Adsorption isotherms

Adsorption isotherms provide useful information such as adsorption mechanism, adsorbate-adsorbent affinity and surface properties. The removal of Cu (II) and Cr (VI) ions using ZnO, Fe<sub>3</sub>O<sub>4</sub> and the ZnO/Fe<sub>3</sub>O<sub>4</sub> nanocomposite as adsorbents were studied with different adsorption isotherm models (Langmuir, Freundlich, Temkin and Dubinin-Radushkevish). According to the Langmuir isotherm, heavy metals adsorb in monolayers on a homogenous surface with a uniform affinity for the adsorbate.<sup>[38]</sup> The dimensionless constant (R<sub>L</sub>) is an equilibrium parameter used to evaluate the important properties of the Langmuir isotherm<sup>[39]</sup> as shown in Eq. (7). Based on the (R<sub>L</sub>) values, adsorption can be characterized as R<sub>L</sub> < 1, linear, R<sub>L</sub> = 1, unfavorable, R<sub>L</sub> > 1, and when R<sub>L</sub> = 0 the adsorption is irreversible. In line with the Freundlich isotherm model, metal ion uptake occurs on a surface that is heterogeneous and has an unequal distribution of adsorption heat.<sup>[38]</sup> The Dubinin-radushkevish model is useful for determining adsorption's apparent energy, which predicts the kind of adsorption (physical or chemical). Temkin isotherm considers indirect adsorbate-adsorbent interactions. Temkin found that the heat of adsorption reduces as coverage increases. Table 1 shows the equations for all the adsorption isotherms.

Equation 6 defines the separation factor (R<sub>L</sub>).

$$R_L = \frac{1}{1 + K_L C_e} \quad (7)$$

### Kinetic models

Adsorption kinetics gives insight into the sorption mechanism, which involves reaction, mass transfer, and diffusion on the surface of the nanoadsorbent, as well as the reaction rate.

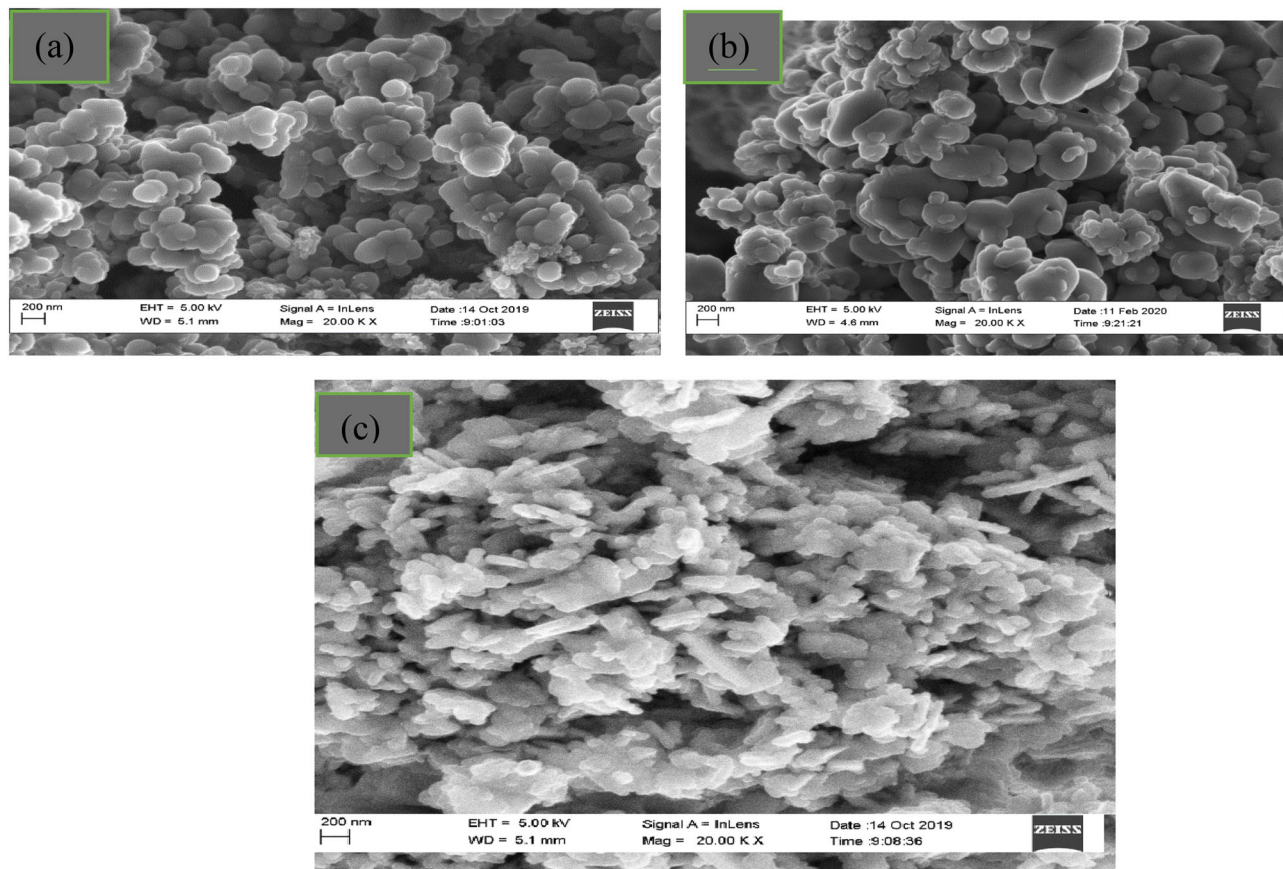
Four different kinetic models were tried to evaluate the mechanism of Cu (II) and Cr (VI) ions adsorption onto ZnO, Fe<sub>3</sub>O<sub>4</sub> nanoparticles and ZnO/Fe<sub>3</sub>O<sub>4</sub> nanocomposite. Kinetic equations for the pseudo-first-order model, pseudo-second-order model, Elovich model, and intraparticle diffusion model are presented in Table 2. The pseudo-first-order kinetic model assumes that all adsorption occurs on isolated sites with no interaction between the adsorbed.<sup>[40]</sup> The

Table 1. Adsorption isotherm models.

Model	Equation
Langmuir model	$\frac{C_e}{q_e} = \frac{1}{q_{max} K_L} + \frac{C_e}{q_{max}}$ (3)
Freunlich model	$\log q = \log K_f + \frac{1}{n} \log C$ (3) (4)
Temkin model	$q_e = \frac{RT}{b} \ln K_T + \frac{RT}{b} \ln C_e$ (4) (5)
Dubinin-Radushkevish model	$\ln q_e = \ln q_m - K_D R^2$ (6)

Table 2. Adsorption kinetics models.

Models	Equations
Pseudo first order	$\log (q_e - q_t) = \log (q_e) - \frac{K_1}{2.303} \times t$ (8)
Pseudo second order	$\frac{t}{q_t} = \frac{1}{k_2 q_e^2} + \frac{t}{q_e}$ (9)
Intraparticle particle diffusion	$q_t = k_1 t^{0.5} + C$ (10)
Elovich	$qt = \frac{1}{\beta} \ln \alpha \beta - \frac{1}{\beta} \ln (t)$ (11)



**Figure 1.** High-resolution scanning electron microscopy of (a) ZnO, (b) Fe<sub>3</sub>O<sub>4</sub> and (c) ZnO/Fe<sub>3</sub>O<sub>4</sub> nanocomposites.

pseudo-second-order model describes behavior over the whole adsorption range and suggests that chemisorption is the step that determines the rate of adsorption.<sup>[41]</sup> According to the intraparticle diffusion kinetics model, intraparticle diffusion is the rate-determining step in the adsorption process if a straight line is formed from a plot of the amount of metal ions adsorbed vs the square root of the contact period.<sup>[42]</sup> Understanding adsorption between the ZnO, Fe<sub>3</sub>O<sub>4</sub> and ZnO/Fe<sub>3</sub>O<sub>4</sub> and the metal ions better, the Elovich kinetic model was subjected to the experimental results. The Elovich kinetic model explains how chemical reactions (chemisorption) occur in nature.<sup>[43]</sup> Table 2 displays all of the adsorption kinetics' fundamental equations

## Results and discussion

### Morphological evaluation of ZnO, Fe<sub>3</sub>O<sub>4</sub> and ZnO/Fe<sub>3</sub>O<sub>4</sub> nanocomposites

The surface morphology of ZnO, Fe<sub>3</sub>O<sub>4</sub> and ZnO/Fe<sub>3</sub>O<sub>4</sub> nanocomposite were investigated by HRSEM and their corresponding images are shown in Figure 1

The HRSEM images in Figure 1 show similar morphology (spherical) for ZnO (a) and Fe<sub>3</sub>O<sub>4</sub> (b), after the formation of ZnO/Fe<sub>3</sub>O<sub>4</sub> nanocomposites the surface morphology changes from spherical to a mixture of spherical and rod-like structure. The findings support the XRD result in Figure 2(b) which shows the existence of both the Fe<sub>3</sub>O<sub>4</sub> and ZnO nanoparticles in

the ZnO/Fe<sub>3</sub>O<sub>4</sub> nanocomposites. Additionally, the ZnO/Fe<sub>3</sub>O<sub>4</sub> nanocomposites (c) are less agglomerated compared to the ZnO and Fe<sub>3</sub>O<sub>4</sub> nanoparticles in Figure 1(a) and (b). This result suggests that the incorporation of Fe<sub>3</sub>O<sub>4</sub> on the surface of ZnO nanoparticles reduces the agglomeration of the nanoparticles resulting in the formation of porous material of a higher surface area. The larger particle shape can also be linked to the diffusion of Fe into the cell lattice of the ZnO nanoparticles. The less aggregation of surface particles could have originated from the low surface energy during the attractive interaction between the ZnO and Fe<sub>3</sub>O<sub>4</sub> nanocomposites.<sup>[44]</sup>

### XRD analysis of ZnO, Fe<sub>3</sub>O<sub>4</sub> nanoparticles and ZnO/Fe<sub>3</sub>O<sub>4</sub> nanocomposites

The mineralogical phase of the ZnO, Fe<sub>3</sub>O<sub>4</sub> nanoparticles and ZnO/Fe<sub>3</sub>O<sub>4</sub> nanocomposite were assessed by XRD and the result is displayed in Figure 2

Figure 2(a) indicates the presence of ten different diffraction peaks at  $2\theta$  values of 21.70, 24.47, 26.25, 37.64, 46.73, 52.92, 56.36, 58.02, 59.12 and 62.77°. These correspond to the following crystal planes: 100, 002, 101, 102, 110, 103, 200, 112, 201 and 004.<sup>[45]</sup> All of the diffraction peaks associated with ZnO nanoparticles were indexed as a hexagonal wurtzite structure, in which half of the tetrahedral sites are occupied by zinc atoms and the arrangement of oxygen atoms is hexagonally closed. The lattice constants for the peaks are  $a = b = 3.242$  and  $c = 5.205$ , which fit the Joint Committee on

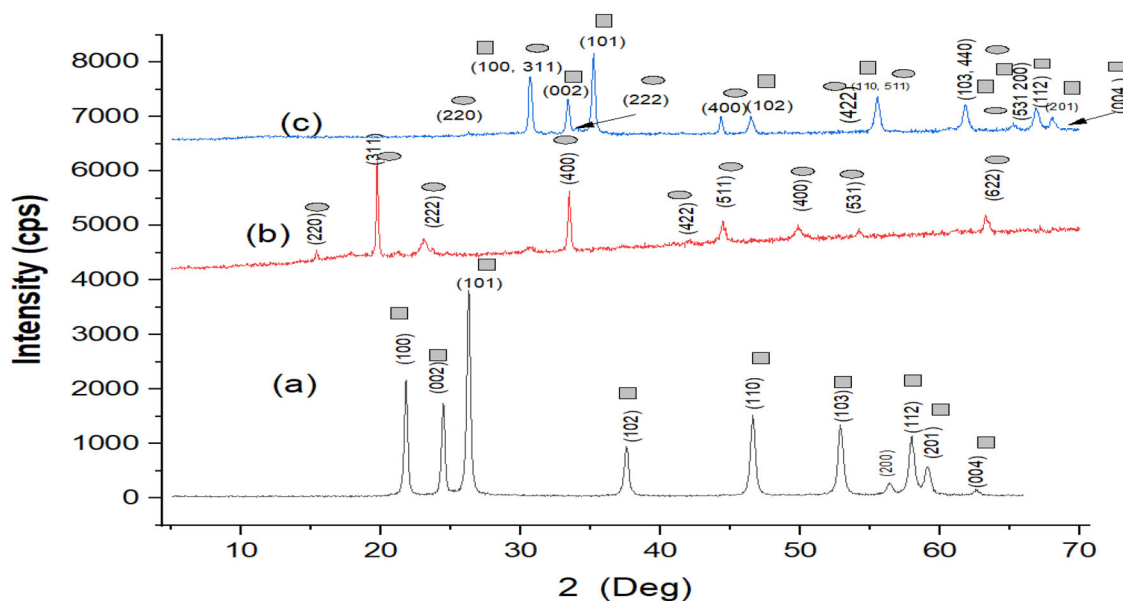


**Figure 2.** XRD of ZnO (a), Fe<sub>3</sub>O<sub>4</sub> (b) nanoparticles and ZnO/Fe<sub>3</sub>O<sub>4</sub> nanocomposites (c).

Powder Diffraction Standards number (JCP2-36-1451). The ZnO nanoparticles was estimated to have a 20.12 nm crystallite size according to the Debye Scherrer equation (see Eq. 11). This result corroborated the research findings by Diallo *et al.*<sup>[46]</sup>. In addition,<sup>[47]</sup> studied the effect of PVP on the synthesis of Fe nanoparticles via chemical reduction using NaBH<sub>4</sub> as a reducing agent and PVP as a capping agent. The authors reported the existence of Fe, Fe<sub>2</sub>O<sub>3</sub>, and Fe<sub>3</sub>O<sub>4</sub>. The existence of Fe and Fe<sub>2</sub>O<sub>3</sub> in their analysis was linked to non-thermal treatment during the process of the synthesis of the nanoparticles. The method employed in this work may be an alternative way to synthesize pure Fe<sub>3</sub>O<sub>4</sub> nanoparticles without the presence of other forms of iron nanoparticles. The possible reaction mechanisms for the synthesis of Fe<sub>3</sub>O<sub>4</sub> using NaBH<sub>4</sub> and PVP were proposed (see Eqs. 11–19). The advantage of this method over the co-precipitation method as reported by<sup>[48,49]</sup> is that the method adopted here shows that Fe<sub>3</sub>O<sub>4</sub> nanoparticles can be synthesized directly using only **iron (III) ion Fe<sup>+3</sup> as a precursor against the use of (Fe<sup>+3+</sup> and Fe<sup>2+</sup> via co-precipitation**. This approach is cost-effective compared to the co-precipitation method.

Figure 2(b) reveals the presence of intense diffraction peaks with the crystal planes of (220), (311), (400), (422), (511), (440), and at 2θ values of 30.56°, 35.86°, 43.46°, 54.01°, 57.38°, 74.46° and (531). The diffraction peaks and the reference magnetite nanoparticles (JCP2-190629) with face-centered cubic structure and a unit cell length of a = 8.396 were in good agreement and conformed to the crystallographic system of the cubic structure of the Fe<sub>3</sub>O<sub>4</sub> nanoparticles. According to Eq. (11), the crystallite size of Fe<sub>3</sub>O<sub>4</sub> nanoparticles was determined to be 26.36 nm.

Figure 2(c) indicates diffraction peaks at 2θ values of 31°, 34°, 36°, 47°, 56°, 62°, 66, 67 and 72°; which correspond to the following crystal planes (100), (002), (101), (102), (110), (103), (200), (112), (201) and (004) reflecting ZnO hexagonal wurtzite. The peaks at (2θ) values of 27.43°, 31.65°, 35.42°, 45.51°, 54.01°, 56.44°, 62.66° and 75.28°, which match the

following crystal planes of (220), (311), (222), (400), (422), (511), (440), and (533), suggest successful immobilization of ZnO wurtzite lattice onto the core shells of Fe<sub>3</sub>O<sub>4</sub>. As shown in Figure 2(b), it was noticed that Fe<sub>3</sub>O<sub>4</sub> nanoparticles in the nanocomposite appeared at lower 2θ values compared to the pure Fe<sub>3</sub>O<sub>4</sub>, which suggests the incorporation of Fe<sub>3</sub>O<sub>4</sub> nanoparticles into the ZnO nanoparticles. The phases of ZnO and Fe<sub>3</sub>O<sub>4</sub> remain unchanged however ZnO dominated with intense peaks while Fe<sub>3</sub>O<sub>4</sub> exhibited a weak diffraction peak with a face-centered cubic phase (JCP2\_40-1141). This is because some of the Fe<sup>2+</sup>/Fe<sup>3+</sup> ions in Fe<sub>3</sub>O<sub>4</sub> nanocomposite were substituted and replaced by O<sup>2-</sup> ions which did not enter the void spaces of ZnO leading to a reduction of the intensity of Fe<sub>3</sub>O<sub>4</sub> in the nanocomposites. The average particle crystallite size of the ZnO/Fe<sub>3</sub>O<sub>4</sub> nanocomposites was 14.50 nm using Debye-Scherrer's equation (see Eq. 11). The decrease in the crystallite size of ZnO/Fe<sub>3</sub>O<sub>4</sub> compared to ZnO and Fe<sub>3</sub>O<sub>4</sub> alone can be explained as follows: Fe ions in ZnO/Fe<sub>3</sub>O<sub>4</sub> matrix exist in the form of Fe<sup>3+</sup> and has a smaller ionic radius of 0.64 Å compared to that of Zn<sup>2+</sup> (0.74 Å) in the composites. The differences in the ionic radius may have resulted in the tensile strain as well as a decrease in the unit cell of the ZnO/Fe<sub>3</sub>O<sub>4</sub> formed, leading to the reduction in the crystallite size of the nanocomposites. A similar trend has been reported by<sup>[50]</sup> for ZnO/Fe<sub>3</sub>O<sub>4</sub> nanocomposite prepared by a combination of sonochemical and sol-gel methods where a mixture of Fe<sub>3</sub>O<sub>4</sub> and α-Fe<sub>2</sub>O<sub>3</sub> nanoparticles appeared in the nanocomposite. The differences observed may be due to the method of synthesis of the nanoparticle and its composites, the nature of the metal salt precursors and the calcination temperature employed. Additionally,<sup>[51]</sup> also reported the formation of high intense diffraction peaks of ZnO compared to Fe<sub>3</sub>O<sub>4</sub> in composites. Also, it was observed from the XRD pattern in Figure 2(a) and (b) that the diffraction peaks for the pure ZnO and Fe<sub>3</sub>O<sub>4</sub> shift toward higher angles of the 2-theta after the formation of the ZnO/Fe<sub>3</sub>O<sub>4</sub> nanocomposites, which is an

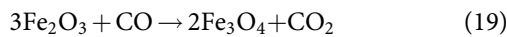
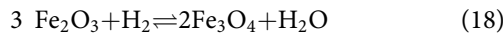
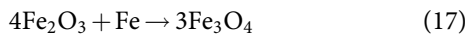
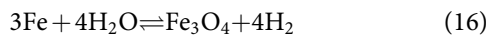
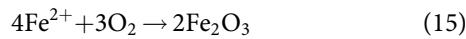
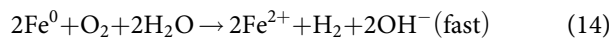
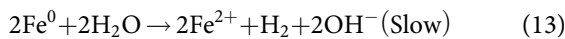
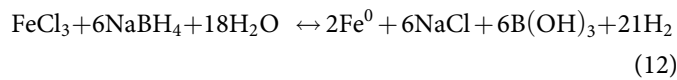


evidence of change of orientation. This could be linked to the differences in the ionic radii ( $\text{Fe}^{2+}$  (0.76 Å) and  $\text{Fe}^{3+}$  (0.64 Å) compared to that of  $\text{Zn}^{2+}$  (0.74 Å)) of the nanoparticles and thus responsible for the change in lattice parameters of the nanoparticles after the formation of the nanocomposites. There is also the possibility of the atoms with smaller atomic radii diffusing into the latticed structure of the other atoms leading to strain.

$$D = \frac{k\lambda}{\beta \cos\theta} \quad (11)$$

The step-by-step reaction mechanism for the formation of  $\text{Fe}_3\text{O}_4$  nanoparticles prepared using Ferric chloride as an iron precursor is shown in Eqs. (12)–(19).

Equation 12 is the reaction between the iron (III) chloride ( $\text{FeCl}_3$ ) and sodium borohydride  $\text{NaBH}_4$  in an aqueous solution to form  $\text{Fe}^0$ .



The  $\text{Fe}^0$  reacts (redox) with ( $\text{H}_2\text{O}$ ) and oxygen ( $\text{O}_2$ ) to form iron (II) oxide ( $\text{Fe}^{2+}$ ) in solution (see Eqs. 13 and 14).

This reaction is faster in the presence of water. The  $\text{Fe}^{2+}$  oxide further reacts with  $\text{O}_2$  and formed of  $\text{Fe}_2\text{O}_3$  (see Eq. 15). The  $\text{Fe}^{3+}$  in the solution that was not completely reduced by the  $\text{NaBH}_4$  further react with  $\text{H}_2\text{O}$  to form magnetite under hydrothermal conditions (see Eq. 16). The  $\text{Fe}_2\text{O}_3$  form could also react with iron metal ( $\text{Fe}$ ) through the hydrothermal process to form  $\text{Fe}_3\text{O}_4$ .

### EDS analysis of ZnO, $\text{Fe}_3\text{O}_4$ nanoparticles and ZnO/ $\text{Fe}_3\text{O}_4$ nanocomposites

The chemical composition of ZnO,  $\text{Fe}_3\text{O}_4$  nanoparticles, and ZnO/ $\text{Fe}_3\text{O}_4$  composites was determined using EDS and the result is given in Figure 3.

Figure 3(a) reveals the existence of Zn, O, and C elements. There is an appearance of the peak corresponding to O at 0.50 keV, Zn at 1.01, 8.65 and 9.49 keV. The percentage concentration for Zn, O and C was 12.24%, 8.99% and 78.77% respectively. The spectra in Figure 3(b) revealed the existence of Fe, O and C. The peak of O was found at 0.54 keV, the Fe signal was shown at 0.72 keV, 6.43 keV, and 7.10 keV while the appearance of C was at 0.29 keV. The percentage concentration was 37.24%, 13.73% and 49.03% for O, C and Fe respectively. Figure 3(c) indicates a very strong peak for Zn (35.03%) ion compared to the Fe (19.68%), this observation may be related to the higher density of Zn (7.134 g/mL) relative to Fe (7.874 g/mL). Based on the density differences, Fe may settle at the bottom with Zn deposited at the surface of the Fe during the synthesis. This result suggests the dominance of the Zn ion over the Fe ion in the composition. This finding is consistent with the observation of<sup>[47]</sup> who reported the elemental composition of Fe (33.08%) and Zn (66.91%) in the formation of ZnO/ $\text{Fe}_3\text{O}_4$  nanocomposite. Another researcher has reported 70.84% and 14.79% for Zn and Fe ions during the formation of ZnO/ $\text{Fe}_3\text{O}_4$  nanocomposites.<sup>[48]</sup>

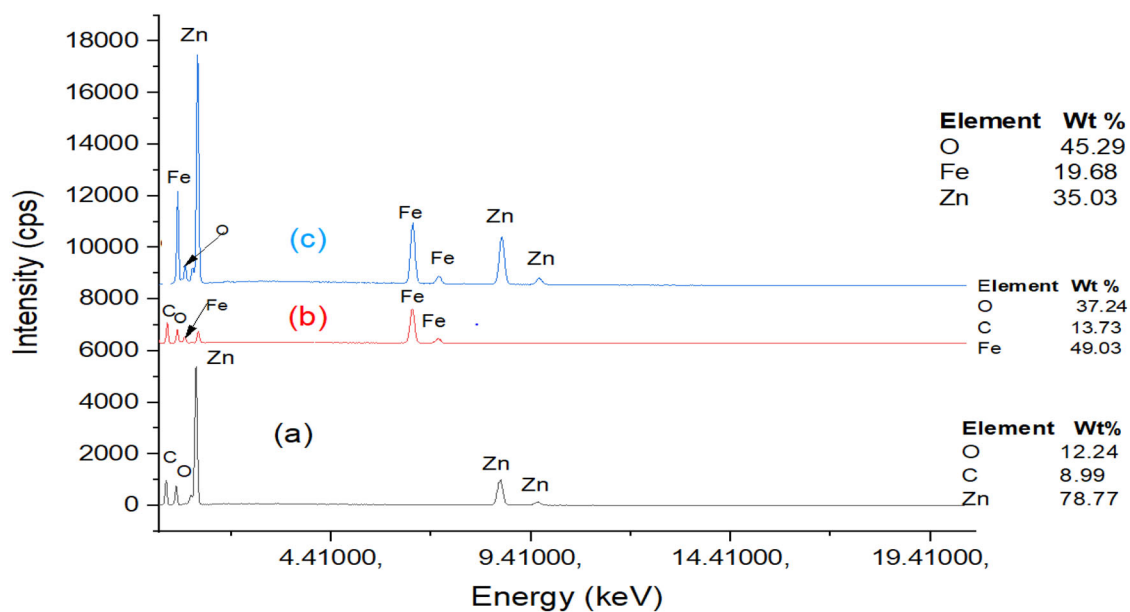


Figure 3. EDS of (a) ZnO, (b)  $\text{Fe}_3\text{O}_4$  and (c) ZnO/ $\text{Fe}_3\text{O}_4$  nanocomposites.



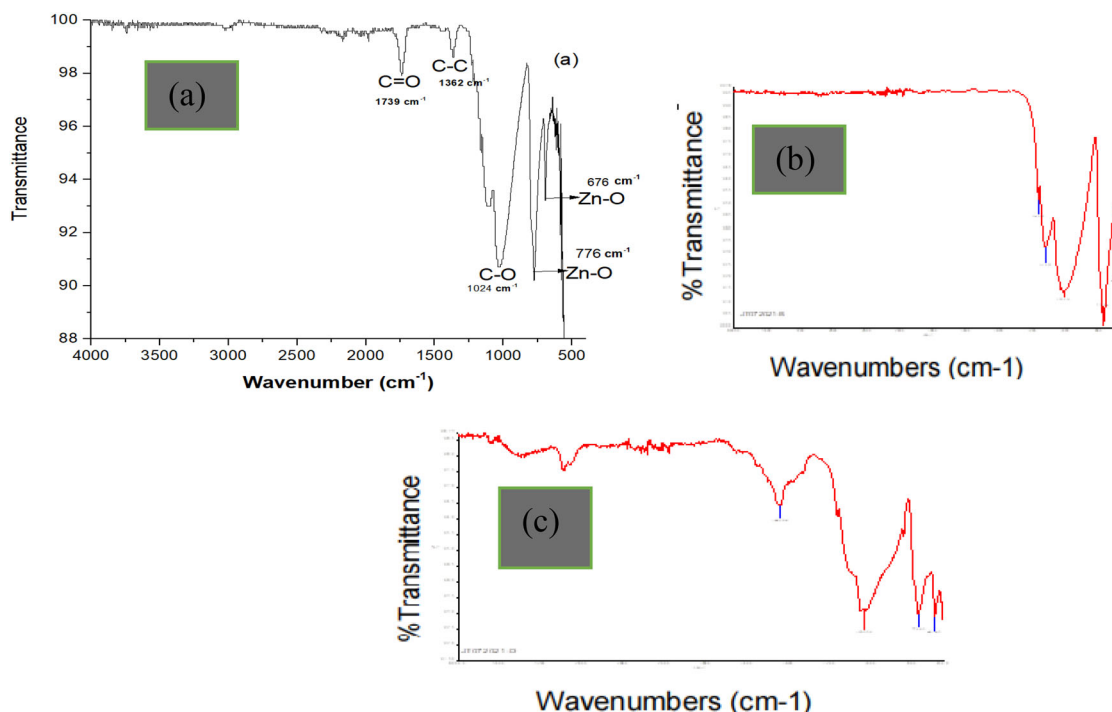


Figure 4. FTIR of (a) ZnO, (b)  $\text{Fe}_3\text{O}_4$  nanoparticles and (c) ZnO/ $\text{Fe}_3\text{O}_4$  nanocomposites.

#### Fourier transforms infrared spectroscopy analysis of ZnO, $\text{Fe}_3\text{O}_4$ nanoparticles and ZnO/ $\text{Fe}_3\text{O}_4$ nanocomposites

FTIR investigation of ZnO,  $\text{Fe}_3\text{O}_4$  nanoparticles and ZnO/ $\text{Fe}_3\text{O}_4$  nanocomposite was done to confirm the presence of the functional groups and the result is given in Figure 4.

Figure 4(a) displays a peak at  $1735\text{ cm}^{-1}$  corresponding to C=O which emanated from the PVP. The peak at  $1358\text{ cm}^{-1}$  signifies the existence of the C-H bond. It is possible that the PVP also causes the vibrations to stretch at  $1110.8\text{ cm}^{-1}$  corresponding to C-N bonds. The C-O stretching is assigned to the peak at  $1024\text{ cm}^{-1}$ .

The peaks around  $692.12$  and  $771.96\text{ cm}^{-1}$  in Figure 4(b) correspond to the Fe-O bond of  $\text{Fe}_3\text{O}_4$  nanocomposites. The vibration bond at  $1119\text{ cm}^{-1}$  is related to the C-O bond, a similar bond has been reported by.<sup>[52]</sup> Another adsorption bond at a wavelength of  $1163\text{ cm}^{-1}$  is linked to the C-O-C bond. Additionally, the adsorption bond at  $1035\text{ cm}^{-1}$  is linked to the N-H stretching and bending vibration of the amine  $\text{NH}_2$  group in the PVP used. The broad peak at  $3447\text{ cm}^{-1}$  is allocated to the O-H stretching vibration of  $\text{H}_2\text{O}$  in ZnO/ $\text{Fe}_3\text{O}_4$  nanocomposite. Other significant peaks at  $1440$  and  $1033\text{ cm}^{-1}$  are related to C-H and C-O bonds. The peaks at  $770\text{ cm}^{-1}$  and  $691\text{ cm}^{-1}$  are linked to microstructural characteristics caused by the addition of  $\text{Fe}_3\text{O}_4$  to the Zn-O lattice to form ZnO/ $\text{Fe}_3\text{O}_4$  nanocomposite. The overlapping of magnetite nanoparticles onto ZnO particles may cause a slight shift in the adsorption bonds.<sup>[53]</sup> This result indicates that the ZnO/ $\text{Fe}_3\text{O}_4$  nanocomposites had more function groups compared to the individual nanoparticles. This is an indication that the ZnO/ $\text{Fe}_3\text{O}_4$  nanocomposite is a better adsorbent compared with the individual nanoparticles due to the availability of various functional groups for binding with the pollutants.

#### BET $\text{N}_2$ adsorption/desorption analysis

The BET  $\text{N}_2$  adsorption-desorption method was used to measure the surface area, pore diameter, and pore volume of ZnO,  $\text{Fe}_3\text{O}_4$ , and ZnO/ $\text{Fe}_3\text{O}_4$  nanocomposite materials. The results obtained are shown in Figure 5.

According to the IUPAC classification, the hysteresis loop of ZnO,  $\text{Fe}_3\text{O}_4$  nanoparticles and ZnO/ $\text{Fe}_3\text{O}_4$  nanocomposites in Figure 5a1, b1 and c1 correspond to type IV isotherm, which is typical of a mesoporous material.<sup>[54]</sup> The similarity between the isotherms, suggests that the materials have similar porous structures.<sup>[55]</sup> The formation of mesoporous structure is further confirmed by the inserted pore size distribution in Figure 5a2, b2 and c2. The pore size distribution for ZnO,  $\text{Fe}_3\text{O}_4$  nanoparticles and ZnO/ $\text{Fe}_3\text{O}_4$  nanocomposites were 26 nm, 18.245 nm and 20 nm respectively. These values fall between 2 and 50 nm for a typical mesoporous material, which is further corroborated by type IV isotherm nanoparticles.<sup>[56]</sup>

Materials with pore diameters between 2 and 50 nm are known as mesoporous materials. These materials have been characterized to have a high surface area, controllable pore diameters, large pore volumes that permit quick adsorption of pollutants, as well as active pore surfaces that are simple to modify or functionalize.<sup>[57]</sup> These qualities satisfy the ideal standards required of a good adsorbent for the treatment of heavy metal-laden wastewater.

According to Table 3, it was found that the surface area of ZnO/ $\text{Fe}_3\text{O}_4$  ( $39.45\text{ m}^2/\text{g}$ ) with a corresponding pore volume of  $0.353\text{ cm}^3/\text{g}$ ,  $4.20\text{ cm}^3/\text{g}$  and  $0.12\text{ cm}^3/\text{g}$  is significantly greater than ZnO ( $8.62\text{ m}^2/\text{g}$ ) and  $\text{Fe}_3\text{O}_4$  ( $7.86\text{ m}^2/\text{g}$ ). The high surface area after the formation of ZnO/ $\text{Fe}_3\text{O}_4$  nanocomposites indicates more active binding sites and free reactive species in ZnO/ $\text{Fe}_3\text{O}_4$  nanocomposites than in ZnO and  $\text{Fe}_3\text{O}_4$ .

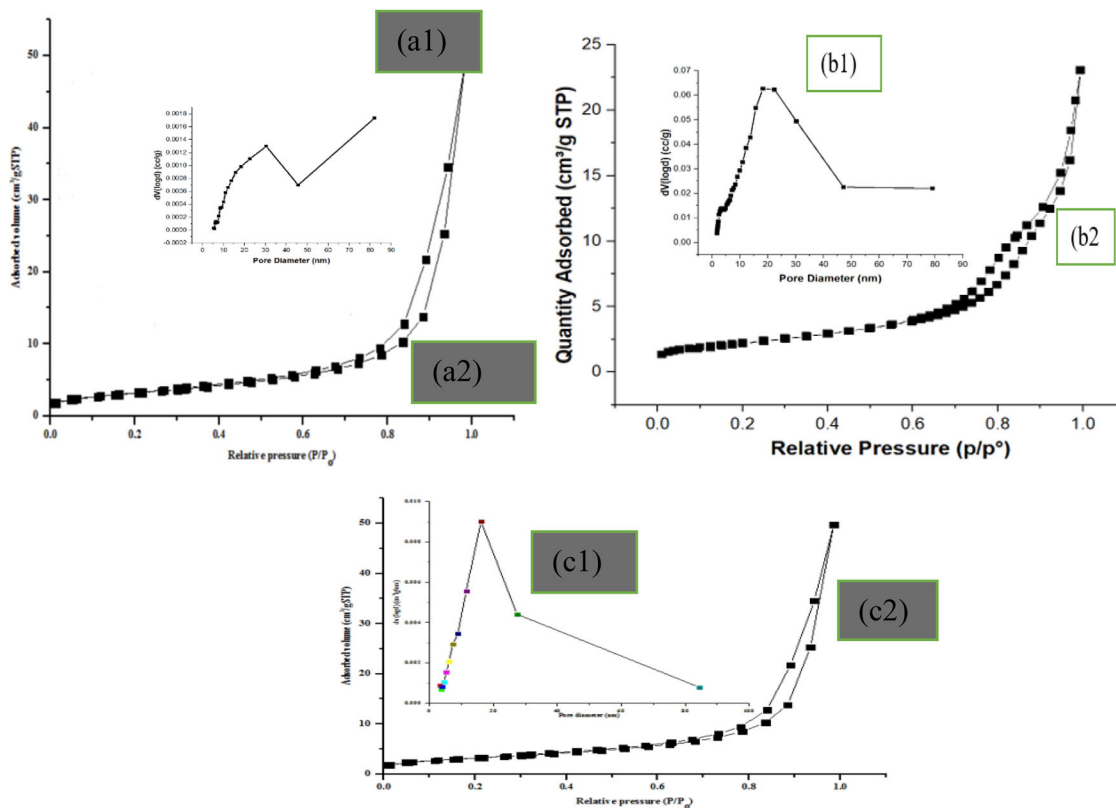


**Figure 5.** ZnO (a1), (b1) and (c1) are nitrogen adsorption-desorption curves and (a2), (b2) and (c2) are pore size diameter distributions for ZnO, Fe<sub>3</sub>O<sub>4</sub> nanoparticles and ZnO/Fe<sub>3</sub>O<sub>4</sub> nanocomposites.

**Table 3.** BET results of ZnO, Fe<sub>3</sub>O<sub>4</sub> nanoparticles and ZnO/Fe<sub>3</sub>O<sub>4</sub> nanocomposite.

Sample	Surface area (m <sup>2</sup> /g)	Pore volume (cm <sup>3</sup> /g)	BJH pore diameter (nm)
ZnO	8.62	0.35	26.17
Fe <sub>3</sub> O <sub>4</sub>	7.86	4.20	18.24
ZnO/Fe <sub>3</sub> O <sub>4</sub>	39.45	0.12	20.54

nanoparticles alone.<sup>[38]</sup> The high surface area obtained for ZnO/Fe<sub>3</sub>O<sub>4</sub> nanocomposites compared to the individual nanoparticles (ZnO and Fe<sub>3</sub>O<sub>4</sub>) may be due to the reduction in the crystallite size after the incorporation of Fe<sub>3</sub>O<sub>4</sub> into the lattice structure of ZnO.<sup>[58]</sup> Have also reported that the surface area of nanoparticles increases with decreasing crystallite size.

### Physico-chemical characteristics of the wastewater from petroleum refinery

Table 4 displays the physicochemical characteristics of petroleum refinery wastewater.

Table 4, demonstrates that the concentration of the pollutants decreases after the adsorption using ZnO, Fe<sub>3</sub>O<sub>4</sub> nanoparticles and ZnO/Fe<sub>3</sub>O<sub>4</sub> nanocomposites as nanoadsorbents. The concentration of COD (mg/L) was  $880.15 \pm 0.30$  before the adsorption and reduced to  $48.03 \pm 0.50$ ,  $50.20 \pm 0.20$  and  $63.712 \pm 0.11$  after treatment by ZnO, Fe<sub>3</sub>O<sub>4</sub> nanoparticles and ZnO/Fe<sub>3</sub>O<sub>4</sub> nanocomposites. The BOD concentration ( $190.32 \pm 0.20$  mg/L), decreased to  $37.41 \pm 0.10$  mg/L,  $48.01 \pm 0.03$  mg/L, and  $52.34 \pm 0.05$  mg/L. The significant reduction in COD and BOD value after treatment with the

nanoadsorbents indicate that the prepared nanoadsorbents can be used to remove organic pollutants from aqueous matrix. The Cu (II) concentration reduced from  $2.98 \pm 0.23$  mg/mL to  $0.305 \pm 0.20$  mg/L,  $0.703 \pm 0.11$  mg/mL,  $0.761 \pm 0.12$  mg/mL. The concentration of Cr (VI) ( $0.59 \pm 0.15$ ) decreased to  $0.203 \pm 0.05$  mg/L,  $0.264 \pm 0.11$  mg/L and  $0.323 \pm 0.10$  mg/L using ZnO, Fe<sub>3</sub>O<sub>4</sub> nanoparticles and ZnO/Fe<sub>3</sub>O<sub>4</sub> nanocomposites. According to Table 3, the nanoadsorbents reduced the conductivity and the pH values within the recommended values. Generally, the ZnO/Fe<sub>3</sub>O<sub>4</sub> nanocomposites had higher removal efficiency for the removal of both Cu (II) and Cr (VI) compared to the use of individual nanoparticles. This may be ascribed to the high surface area of the ZnO/Fe<sub>3</sub>O<sub>4</sub> nanocomposites compared to ZnO and Fe<sub>3</sub>O<sub>4</sub> nanoparticles alone.

### Batch adsorption studies

#### Effect of contact time

Figure 6(a) and (b) depict the removal of Cu (II) and Cr (VI) ions at different times (0 to 25 minutes) using ZnO, Fe<sub>3</sub>O<sub>4</sub> nanoparticles and ZnO/Fe<sub>3</sub>O<sub>4</sub> nanocomposite as nanoadsorbent

Both the removal of Cu (II) and Cr (VI) ions was slow within the first five minutes and thereafter rapidly increased till 10 minutes, then the adsorption efficiency increased at a very slower rate until it achieved equilibrium after 15 minutes of contact using the three nanomaterials. This phenomenon may be attributed to the availability of an enormous number of unoccupied sites at 10 minutes for the adsorption of Cu (II) and Cr (VI) ions from wastewater

**Table 4.** Physico-chemical evaluation of the petroleum refinery wastewater before and after treatment.

Parameter	Before Adsorption	After Adsorption			WHO permissible limit (2017)
		ZnO/Fe <sub>3</sub> O <sub>4</sub>	ZnO	Fe <sub>3</sub> O <sub>4</sub>	
Chemical oxygen demand (COD) mg/L	880.15 ± 0.30	48.03 ± 0.50	50.20 ± 0.20	63.712 ± 0.11	40
Biological oxygen demand (BOD) mg/L	190.32 ± 0.20	37.41 ± 0.10	48.01 ± 0.03	52.34 ± 0.05	1
Copper (Cu) mg/mL	2.98 ± 0.23	0.305 ± 0.20	0.703 ± 0.11	0.761 ± 0.12	0.01
Chromium (Cr) mg/mL	0.59 ± 0.15	0.203 ± 0.05	0.264 ± 0.11	0.323 ± 0.10	0.08
Temperature (°C)	31.20 ± 0.12	31.41 ± 0.12	31.65 ± 0.1	31.32 ± 0.1	30
pH	6.25 ± 0.10	7.02 ± 0.11	6.81 ± 0.11	6.34 ± 0.20	6.51–8.5
Electrical conductivity (μS/cm)	483.74 ± 0.13	63.23 ± 0.04	76.03 ± 0.13	80.00 ± 0.121	–

Key: WHO = World Health Organization.

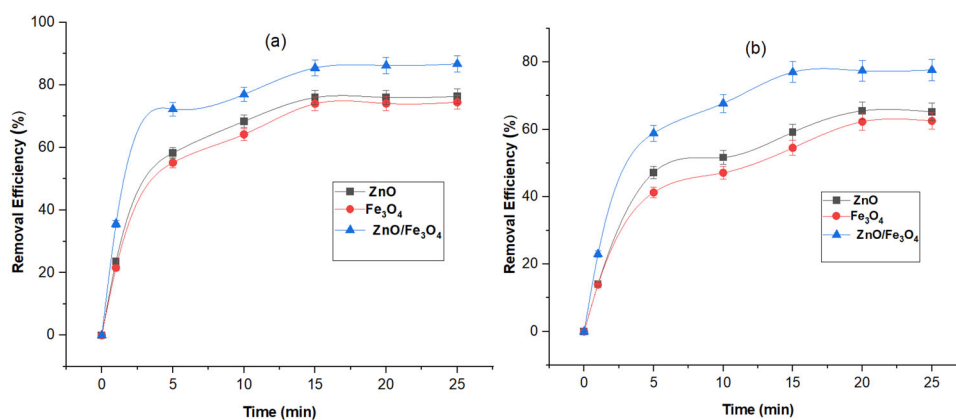


**Figure 6.** Effect of contact time on the elimination of Cu (II) (a) and Cr (VI) ions (b) at adsorbent dose (0.05 g), volume of the petroleum wastewater (50 mL), pH (6.25) and temperature (30 °C).

from petroleum refinery wastewater. The highest removal efficiency was in the order of Cu (II) (76.4%, 74.47%, and 86.76%) > Cr (VI) (65.19%, 62.53% and 77.65%) for ZnO, Fe<sub>3</sub>O<sub>4</sub> and ZnO/Fe<sub>3</sub>O<sub>4</sub> nanocomposites respectively. The high percentage removal of Cu (II) and Cr (VI) ions occurred using ZnO/Fe<sub>3</sub>O<sub>4</sub> nanocomposite may be due to its large surface area (Table 2) and small crystallite size than ZnO and Fe<sub>3</sub>O<sub>4</sub> nanoparticles alone. Furthermore, the increase adsorptive capacity of ZnO than the Fe<sub>3</sub>O<sub>4</sub> nanoadsorbent could be attributed to the additional active functional groups present in ZnO nanoparticles compared to Fe<sub>3</sub>O<sub>4</sub> nanoparticles. The high removal of Cu (II) ion compared to Cr (VI) ion by the nanoadsorbents at every contact time may be correlated to its smaller atomic radii of Cu (II) (1.657 Å) than Cr (VI) (2.778 Å) ions. This suggests that the higher the ionic radii the lower the removal efficiency of the metal ions because higher ionic radii generate more steric congestion and cause faster saturation of the adsorption sites, which hinder the movement of the ions from the aqueous phase to the nanoadsorbent surface.<sup>[16]</sup>

#### Effect of adsorbent dose

The effect of the nanoadsorbent dosage on the adsorption of Cu (II) and Cr (VI) ions from petroleum refinery wastewater was examined at different dosages (0.02, 0.04, 0.06, 0.08, 0.1 to 0.12 g/50 mL) and the result obtained is displayed in Figure 7(a) and (b)

According to Figure 7, the adsorption removal efficiency increases as the adsorbent dose increases, and maximum

removal efficiency was attained at 0.08 g/50 mL. The availability of more binding sites may be responsible for the increase in the percentage adsorption efficiency as the nanoadsorbent dosage increases.<sup>[58]</sup> The highest removal efficiency for Cu (II) ion were 83.86%, 80.57%, and 90.99% while that of Cr (VI) were 64.34%, 61.00% and 77.60%. There was no notable increase in the elimination of Cu (II) and Cr (VI) after 0.08 g/50 mL. The percent removal remained unchanged because the available adsorption sites were saturated and further increase did not lead to any notable adsorption. The high adsorption behavior of ZnO/Fe<sub>3</sub>O<sub>4</sub> nanocomposites compared with ZnO and Fe<sub>3</sub>O<sub>4</sub> nanoparticles may be associated with the existence of additional functional groups and higher surface area in the former than in the latter.

#### Effect of temperature

The results of the effect of temperature on the adsorption of Cu (II) and Cr (VI) ions from wastewater from petroleum refinery are presented in Figure 8(a) and (b):

Figure 8(a) and (b) reveal that the adsorption efficiency of Cu (II) and Cr (VI) ions by ZnO, Fe<sub>3</sub>O<sub>4</sub> nanoparticles and ZnO/Fe<sub>3</sub>O<sub>4</sub> nanocomposites increases as the temperature increases, this rise in Cu (II) and Cr (VI) adsorption efficiency may be linked to the creation of more active sites as a result of the breakage of some internal bonds, as well as the edges of the nanoadsorbents, at high temperatures.<sup>[59]</sup> The increase in reaction temperature also caused an increase in energy, resulting in high solubility and mobility of ions. The increase in reaction temperature also lead to an increase in the swelling of the

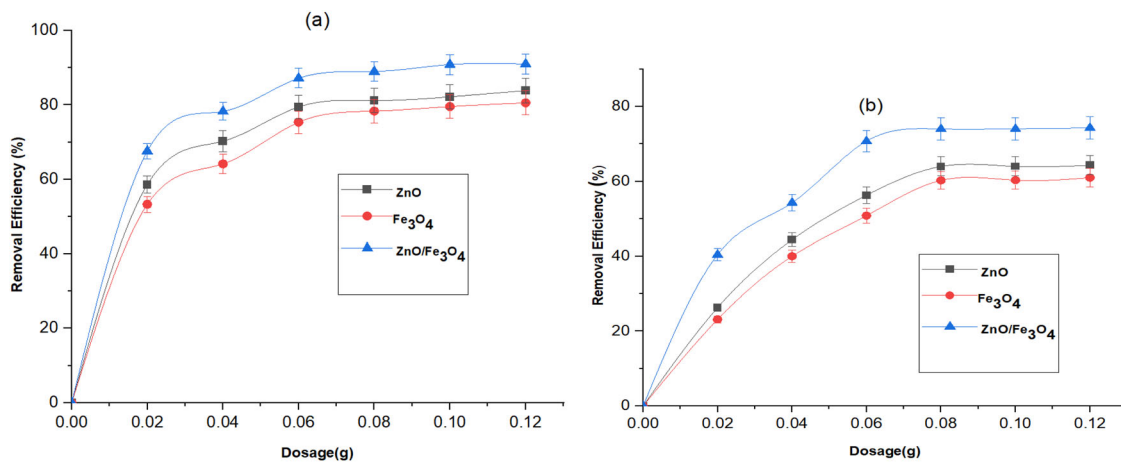


**Figure 7.** Removal of (a) Cu (II) (b) and Cr (VI) using different nanoadsorbent at volume of the petroleum wastewater (50 mL), pH (6.25), temperature (30 °C) and contact time (15 min).

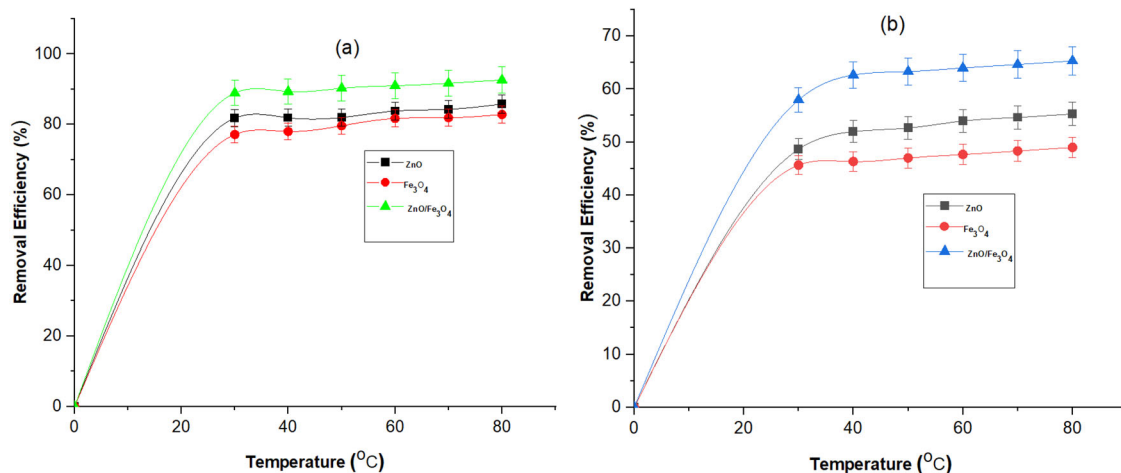


**Figure 8.** Effect of temperature on the removal of (a) Cu (II) and (b) Cr (VI) at pH (6.25), volume of the petroleum wastewater (50 mL), contact time (15 min) and nanoadsorbent dosage (0.05 g).

interior content of the adsorbent and adsorbate's capacity to penetrate the adsorbent.<sup>[60]</sup> The increase in removal efficiency as a function of temperature confirmed that the adsorption process is endothermic.<sup>[61]</sup> Figure 8 shows that the highest adsorptive efficiency of Cu (II) and Cr (VI) ions using ZnO, Fe<sub>3</sub>O<sub>4</sub> nanoparticles and ZnO/Fe<sub>3</sub>O<sub>4</sub> nanocomposites were 85.83%, 82.86% and 92.67%; 55.33%, 49.00% and 65.33% at 40 °C. The high adsorption of ZnO/Fe<sub>3</sub>O<sub>4</sub> nanocomposites compared with the individual nanoparticles indicates more functional groups after the formation of the nanocomposites, and more complexation between the adsorbate and the adsorbent through coordinate and electrostatic interaction.<sup>[62]</sup> Furthermore, the high performance of ZnO/Fe<sub>3</sub>O<sub>4</sub> nanocomposites than the individual nanoparticles could be ascribed to the large surface area of the nanocomposite.

### Adsorption isotherm

Various isotherm models (Freundlich, Langmuir, Temkin, and Dubinin-rasdushkevish (D-R)) were used to test the equilibrium data for Cu (II) and Cr (VI) ions adsorption

onto ZnO, Fe<sub>3</sub>O<sub>4</sub> nanoparticles and ZnO/Fe<sub>3</sub>O<sub>4</sub> and the results are shown in Table 5.

Table 5 shows that the adsorption data fitted more closely to Langmuir isotherm model due to its highest correlation coefficient ( $R^2$ ) values which range between 0.998 to 0.999 compared with the 0.953-0.998, 0.941-0.990, 0.894-0.957 obtained for Freundlich, Temkin and D-R isotherm using ZnO nanoparticles as an adsorbent. A similar trend was observed for Fe<sub>3</sub>O<sub>4</sub> nanoparticles and ZnO/Fe<sub>3</sub>O<sub>4</sub> nanocomposites.

As a result, the Langmuir model was more suitable for explaining Cu (II) and Cr (VI) adsorption by ZnO, Fe<sub>3</sub>O<sub>4</sub> nanoparticles and ZnO/Fe<sub>3</sub>O<sub>4</sub> nanocomposites. This also demonstrates that mechanisms of the adsorption are monolayer in nature and the chemisorption phenomenon dominated the adsorption process. The highest adsorption capacity ( $q_{max}$ ) values for Cu (II) were (44.948 mg/g, 35.024 mg/g, 46.955 mg/g); and Cr (VI) were (14.539 mg/g, 13.736 mg/g, 23.766 mg/g) using ZnO, Fe<sub>3</sub>O<sub>4</sub> nanoparticles and ZnO/Fe<sub>3</sub>O<sub>4</sub> nanocomposites respectively. This result indicates that the ZnO/Fe<sub>3</sub>O<sub>4</sub> nanocomposites performed better than ZnO and Fe<sub>3</sub>O<sub>4</sub> nanoparticles due to the presence of more binding sites, functional groups and the large surface area of



**Table 5.** Adsorption isotherms for the removal of Cu (II) and Cr (VI) ions.

Model	Parameters	Cu (II)			Cr (VI)			
		ZnO	Fe <sub>3</sub> O <sub>4</sub>	ZnO/Fe <sub>3</sub> O <sub>4</sub>	ZnO	Fe <sub>3</sub> O <sub>4</sub>	ZnO/Fe <sub>3</sub> O <sub>4</sub>	
Langmuir	$q_{\max}$ (mg/g)	44.948	35.024	46.955	14.539	13.736	23.766	
	$K_L$	4.921	4.768	8.010	0.246	0.163	0.420	
	$R_L$	0.028	0.029	0.018	0.295	0.357	0.024	
	$R^2$	0.999	0.998	0.999	0.997	0.995	0.999	
	SSE	0.052	0.053	0.127	0.057	0.056	0.209	
	$\chi^2$	0.432	0.437	0.043	1.414	1.083	0.141	
Freundlich	$K_F$ (mg g <sup>-1</sup> )	1.774	1.487	1.929	1.673	1.406	2.097	
	1/n	0.343	0.409	0.311	0.735	0.868	0.553	
	$R^2$	0.956	0.953	0.993	0.995	0.994	0.998	
	SSE	0.186	0.198	0.186	0.389	0.407	0.389	
	$\chi^2$	0.284	0.295	0.284	1.101	1.139	1.101	
	$K_T$ (L mg <sup>-1</sup> )	0.795	0.575	1.131	0.795	0.575	1.131	
Temkin	$B$ (J/mol)	1972.140	1395.420	1428.700	805.616	755.076	951.753	
	$R^2$	0.941	0.941	0.990	0.941	0.941	0.989	
	SSE	0.076	0.081	0.008	0.080	0.081	0.023	
	$\chi^2$	0.270	0.292	0.124	0.237	0.247	0.187	
	D-R	$q_{\max}$ (mgg <sup>-1</sup> )	19.747	20.890	22.106	2.903	3.642	5.063
		$B_D$ (mol kJ <sup>-2</sup> )	988.710	493.530	1552.470	3309.480	2992.650	3787.410
$E$ (kJ mol <sup>-1</sup> )		1.274	1.275	0.990	1.439	1.460	0.989	
$R^2$		0.896	0.895	0.955	0.894	0.893	0.957	
SSE		0.555	0.560	0.243	1.537	1.206	0.943	
$\chi^2$		6.989	7.221	3.068	18.330	14.671	10.709	

ZnO/Fe<sub>3</sub>O<sub>4</sub> nanocomposites compared to ZnO and Fe<sub>3</sub>O<sub>4</sub> nanoparticles. The high adsorptive capacity of Cu (II) ions compared to that of Cr (VI) ions may be ascribed to their electronegativity value. For instance, Cu (II) ions have a higher electronegativity of 1.94 compared to that of Cr (VI) ions (1.66) resulting in the high removal efficiency of Cu (II) ions compared to the Cr (VI) ion. Additionally, it has been reported that heavy metal ions with a high electronegativity have a considerable attraction for the oxygen atoms' electron cloud in the ZnO, Fe<sub>3</sub>O<sub>4</sub> nanoparticles and ZnO/Fe<sub>3</sub>O<sub>4</sub>.<sup>[63,64]</sup> Who investigated the elimination of Ni (II), Cr (VI), Cu (II), Pb (II), Cd (II) and Zn, (II) ions from the aqueous phase, noticed a similar pattern. The author ascribed the high adsorption capacity of Pb (II) to the higher electronegativity of Pb (II) compared with that of other heavy metals. Another researcher<sup>[63]</sup> has reported that higher electronegativity favors the adsorption of heavy metals.

According to Table 5, the dimensionless ( $R_L$ ) value for Cu (II) ion adsorption from petroleum refinery wastewater using ZnO, Fe<sub>3</sub>O<sub>4</sub> nanoparticles and ZnO/Fe<sub>3</sub>O<sub>4</sub> were (0.028, 0.029 and 0.018) while that obtained for Cr (VI) were: (0.295, 0.357 and 0.024). The value obtained is less than one (1) irrespective of the nano-adsorbent used, signifying that the adsorption process was favorable. The smallest value lower  $R_L$  value (0.018 and 0.24) was obtained for ZnO/Fe<sub>3</sub>O<sub>4</sub> nanocomposites for both Cu (II) and Cr (VI) ion sequestration in comparison to the individual nanoparticles indicating more favorable adsorption of heavy metals using ZnO/Fe<sub>3</sub>O<sub>4</sub> nanocomposites.

The value of  $K_L$  is a parameter for evaluating the affinity between the adsorbent and adsorbate and the values are shown in Table 5. The greater the value of  $K_L$ , the higher the attraction between the nano-adsorbent and Cu (II) and Cr (VI) ions in the solution. In Table 5, it was observed that ( $K_L$ ) values for the elimination of Cu (II) ion were 4.921, 4.768, and 8.010 while that of Cr (VI) ion were 0.246, 0.163

and 0.420 using ZnO, Fe<sub>3</sub>O<sub>4</sub> nanoparticles and ZnO/Fe<sub>3</sub>O<sub>4</sub> nanocomposites as adsorbent. Cu (II) has a greater affinity for ZnO/Fe<sub>3</sub>O<sub>4</sub> nanocomposites (8.010) compared to 4.921 and 4.768 obtained for ZnO and Fe<sub>3</sub>O<sub>4</sub> nanoparticles. Similarly, ZnO/Fe<sub>3</sub>O<sub>4</sub> nanocomposites have a greater affinity for Cr (VI) (0.420) compared to 0.246 and 0.163 obtained for ZnO and Fe<sub>3</sub>O<sub>4</sub> nanoparticles. The high affinity of ZnO/Fe<sub>3</sub>O<sub>4</sub> nanocomposites toward Cu (II) and Cr (VI) ions compared to the individual nanoparticles may be due to the presence of additional adsorption binding sites upon the production of ZnO/Fe<sub>3</sub>O<sub>4</sub> nanocomposites. The result indicates that the Cu (II) ion has a stronger attraction to all the adsorbents than Cr (VI) ion. This may be caused by variations in the atomic radius of Cu (II) and Cr (VI) ions; the higher the atomic radius of the cation, the higher the influence on binding site competition during the adsorption process; thus, Cu (II) ions (1.57 Å) are more influential than Cr (VI) ions (0.53 Å). Smaller ions have been reported to be highly hydrated and then become bulkier than larger ions.<sup>[64]</sup> This increases their chances of being absorbed to the surface of the adsorbent sites earlier than the highly hydrated ions that slowly migrate from the aqueous solutions.

Table 5 displays the Freundlich isotherm models with parameters such as the distribution coefficient for adsorption ( $K_F$  (mg/g)), which represents the quantity of Cu (II) and Cr (VI) adsorbed on the surface of ZnO, Fe<sub>3</sub>O<sub>4</sub> and ZnO/Fe<sub>3</sub>O<sub>4</sub> nanocomposites. The  $K_F$  value for Cu (II) ions were 1.774, 1.487 and 1.929 and that of Cr (VI) ions were 1.673, 1.406 and 2.097 for ZnO, Fe<sub>3</sub>O<sub>4</sub> and ZnO/Fe<sub>3</sub>O<sub>4</sub> respectively. The result indicates that ZnO/Fe<sub>3</sub>O<sub>4</sub> nanocomposites show a higher value for both Cu (II) and Cr (VI) ions. This could be related to the smaller crystallite size of the ZnO/Fe<sub>3</sub>O<sub>4</sub> (14.50 nm) nanocomposites compared to ZnO (20.12 nm), Fe<sub>3</sub>O<sub>4</sub> (26.36 nm) nanoparticles as earlier reviewed by the XRD result.

Table 5 shows that the 1/n value in the case of the Freundlich isotherm model was less than one for both Cu

(II) and Cr (VI). This confirmed the favourability of the removal of Cu (II) and Cr (VI) using ZnO, Fe<sub>3</sub>O<sub>4</sub> and ZnO/Fe<sub>3</sub>O<sub>4</sub> nanocomposite.<sup>[65]</sup> The value of (1/n) is less than one as presented in Table 5, showing that the adsorption between the adsorbate and the adsorbent is a normal Langmuir isotherm,<sup>[66]</sup> since 1/n less than one implies a normal Langmuir isotherm, whereas when 1/n is bigger than 1, cooperative adsorption is established (Freundlich isotherm). This observed trend supports the earlier claims of (R<sup>2</sup>) and R<sub>L</sub> values that the removal of the target pollutants using ZnO/Fe<sub>3</sub>O<sub>4</sub> nanocomposites, ZnO and Fe<sub>3</sub>O<sub>4</sub> nanoparticles are monolayer and chemisorption in nature. To distinguish between physisorption and chemisorption adsorption, the D-R isotherm was employed. According to the D-R isotherm model, chemisorption occurs when the free energy of adsorption (E) is larger than 16 kJ/mol and physisorption adsorption occurs when E ranges from 1 and 16 kJ/mol.<sup>[67]</sup> For the selected heavy metals removed by the nanoadsorbents, the value of (E) obtained in this study is greater than 16 kJ/mol, which implies that chemisorption occurs during the elimination of Cu (II) and Cr (VI) ion using ZnO, Fe<sub>3</sub>O<sub>4</sub> and ZnO/Fe<sub>3</sub>O<sub>4</sub> nanoadsorbent. This result corroborated the thermodynamic and kinetics data where the adsorption of the heavy metals regardless of the adsorbent utilized shows a positive enthalpy value.

The isotherm models were subjected to different error analyses such as the sum of squared errors (SSE) and chi-square (x<sup>2</sup>) since in some circumstances, the correlation coefficient (R<sup>2</sup>) is not adequate to characterize the model fitting. It has been reported that the values of X<sup>2</sup> and SSE error analysis would be small if the values model data is similar to experimental data, and vice versa.<sup>[65]</sup> Based on the result shown in Table 5, the R<sup>2</sup> for both Cu (II) and Cr (VI) ion for Langmuir isotherms was higher than the other models for all the nanoadsorbents indicating the fitness of the adsorption process to the Langmuir Isotherm as earlier reported. Table 5 shows that the values of x<sup>2</sup> and SSE of Langmuir isotherm were lower than the values of Freundlich, Temkin and D-R isotherm for Cu (II) and Cr (VI) ion adsorption irrespective of the nanoadsorbent used. This confirmed the fitness of the Langmuir isotherm model to the other models. The obtained results show that the nanoadsorbents were effective for the treatment of petroleum refinery wastewater under the applied conditions. Various researchers have studied the elimination of Cu (II) and Cr (VI) ions and confirmed the monolayer nature of the adsorption process using different nanoparticles and nanocomposites. For instance,<sup>[31]</sup> studied the elimination of Cu (II) using composites of ZnO/hollow fiber. The authors reported the fitness of the removal process of Cu (II) ions using ZnO/hollow fiber to the Langmuir isotherm (Chemical adsorption). Similarly, the report on the elimination of Cr (VI) ion using ZnO/graphene oxide from an aqueous phase by<sup>[67]</sup> revealed that the Langmuir isotherm is ideal for removing Cr (VI). These results support the conclusion that monolayer adsorption occurs during the adsorption of Cu (II) and Cr (II).

## Adsorption kinetics

The simultaneous elimination of Cu (II) and Cr (VI) ions from petroleum refinery wastewater using Fe<sub>3</sub>O<sub>4</sub>, ZnO and ZnO/Fe<sub>3</sub>O<sub>4</sub> was investigated using various kinetics models and the results are presented in Table 6.

According to Table 6, the R<sup>2</sup> values derived for pseudo first kinetic model using ZnO, Fe<sub>3</sub>O<sub>4</sub> nanoparticles and ZnO/Fe<sub>3</sub>O<sub>4</sub> nanocomposites for the adsorption of Cu (II) were (0.888, 0.853 and 0.898); while for Cr (VI) the values were (0.773, 0.721 and 0.886. These values were lower than (R<sup>2</sup>) of Cu (II) (0.998, 0.998 and 0.999); Cr (VI) (0.990, 0.983 and 0.993) for the pseudo-second-order model. Thus, the experimental data for the removal of Cu (II) and Cr (VI) ions from ZnO, Fe<sub>3</sub>O<sub>4</sub> nanoparticles, and ZnO/Fe<sub>3</sub>O<sub>4</sub> nanocomposites best fits the pseudo-second-order than the pseudo-first-order model. This demonstrates that chemical adsorption dominates the adsorption process and the adsorption process fitted into the pseudo-second order kinetic model.<sup>[25]</sup> Table 6 shows that the values of the (k<sub>2</sub>) using ZnO, Fe<sub>3</sub>O<sub>4</sub> nanoparticles and ZnO/Fe<sub>3</sub>O<sub>4</sub> nanocomposites for the adsorption of Cu (II) were 2.269, 2.215, and 2.447 mg/g·min; Cr (VI) (2.287, 2.046 and 2.726 mg/g·min), which is higher than; 0.188, 0.182 and 0.196 mg/g·min; 0.175, 0.166 and 0.193 mg/g·min for (k<sub>1</sub>) values. The high k<sub>2</sub> recorded for Cu (II) compared to Cr (VI) may be linked to the easy transfer of Cu (II) from the aqueous phase to the surface of the ZnO, Fe<sub>3</sub>O<sub>4</sub> nanoparticles and ZnO/Fe<sub>3</sub>O<sub>4</sub> nanocomposites, leading to the formation of more chemical bonds.

The high values of (k<sub>2</sub>) compared to the values of the (k<sub>1</sub>) for ZnO, Fe<sub>3</sub>O<sub>4</sub> nanoparticles and ZnO/Fe<sub>3</sub>O<sub>4</sub> nanocomposites indicates that the rate of removal of Cu (II) and Cr (VI) ions from the petroleum refinery wastewater was faster for pseudo-second-order compared to the pseudo-first-order kinetics. This further supports the fact that the reaction fits better to pseudo-second order. Comparatively, the ZnO/Fe<sub>3</sub>O<sub>4</sub> nanocomposites have higher values of (R<sup>2</sup>), (k<sub>1</sub> and k<sub>2</sub>) and (q<sub>e1</sub> and q<sub>e2</sub>) followed by ZnO nanoparticles while Fe<sub>3</sub>O<sub>4</sub> nanoparticles recorded the smallest value of (R<sup>2</sup>), (k<sub>1</sub> and k<sub>2</sub>) and (q<sub>e1</sub> and q<sub>e1</sub>) for Cu (II) and Cr (VI) ions.

This demonstrates that the ZnO/Fe<sub>3</sub>O<sub>4</sub> nanocomposites were more efficient in the removal of Cu (II) and Cr (VI) ions from petroleum refinery wastewater due to their higher surface area compared to ZnO and Fe<sub>3</sub>O<sub>4</sub> nanoparticles.

To validate the fitness of the adsorption of Cu (II) and Cr (VI) the data were subjected to different error functions such as chi-square (x<sup>2</sup>) and the sum of squared error (SSE). The values presented in Table 6 indicate that the x<sup>2</sup> for pseudo-second-order kinetics was small for Cu (II) and Cr (VI) irrespective of the adsorbent used. This result supports the fact that the process was governed purely by chemisorption. Similarly, the SSE values for the pseudo-second-order model were lower compared to pseudo-first order, this also confirms the fact that the adsorption was chemical adsorption. It is essential to note that the chi-square (x<sup>2</sup>) value and the sum of squared error (SSE) for ZnO/Fe<sub>3</sub>O<sub>4</sub> nanocomposites was lower than the values obtained for ZnO and Fe<sub>3</sub>O<sub>4</sub> nanoparticles. This is another confirmation that the

ZnO/Fe<sub>3</sub>O<sub>4</sub> nanoadsorbent performed better than ZnO and Fe<sub>3</sub>O<sub>4</sub> nanoparticles for both Cu (II) and Cr (VI).

To understand the adsorption mechanisms, other kinetic models such as the Elovich and intraparticle diffusion were employed. Table 6 shows that the (R<sup>2</sup>) for the intraparticle diffusion ranges from 0.679 to 0.918, comparing these values with the earlier reported values for the pseudo-first-order (0.721-0.898) and pseudo-second-order (0.990 to 0.999) kinetic models, it means that the removal of Cu (II) and Cr (VI) ions using the three nanoadsorbents from the petroleum refinery wastewater was not governed by intraparticle diffusion kinetic model. The k<sub>id</sub> (g/min) values were found to be higher for ZnO/Fe<sub>3</sub>O<sub>4</sub> nanocomposites compared with ZnO and Fe<sub>3</sub>O<sub>4</sub> nanoparticles which could be as a result of the stronger driving force between the pollutants and ZnO nanoparticles. This result justifies the high efficiency of ZnO/Fe<sub>3</sub>O<sub>4</sub> nanocomposites over ZnO and Fe<sub>3</sub>O<sub>4</sub> nanoparticles.

Additionally, it has been reported that the plot of qt against t<sup>0.5</sup> should be linear and pass through the origin if the intraparticle diffusion kinetic model governed the adsorption process.<sup>[68]</sup> The plots of qt against t<sup>0.5</sup> are linear and did not pass through the origin. This deviation strongly suggests that the intraparticle diffusion kinetic model was not the rate-controlling step during the adsorption of Cu (II) and Cr (VI) from the petroleum refinery wastewater, but other kinetic models may simultaneously control the adsorption rate.

The Elovich kinetics model is one of the most helpful models for understanding chemisorption. Table 6 indicates that the R<sup>2</sup> ranges between 0.661 to 0.898, this result further supports the earlier claim that the removal process is chemisorption.<sup>[69]</sup> The pseudo-second-order kinetic model had R<sup>2</sup> closer to 1 when compared to intraparticle diffusion, Elovich and pseudo-first-order kinetic models. This suggests that the removal of Cu (II) and Cr (VI) ions irrespective of nanoadsorbent used was more accurately explained by a pseudo-second-order kinetic model.

### Thermodynamics

The thermodynamics study for the removal of Cu (II) and Cr (VI) ions using ZnO, Fe<sub>3</sub>O<sub>4</sub> and ZnO/Fe<sub>3</sub>O<sub>4</sub> composites were investigated to predict the feasibility of the adsorption process. Standard enthalpy change (ΔH°) and standard entropy change (ΔS°) were determined from the slope and intercept of the linear plot of lnK<sub>d</sub> versus 1/T as presented in Eq. (12). Equation 13 was used to calculate the standard Gibb's free energy change (ΔG°), and the result is presented in Table 7.

$$\Delta G^\circ = -RT \ln K_d \tag{20}$$

$$\ln K_d = \frac{(\Delta S^\circ)}{R} - \frac{(\Delta H^\circ)}{RT} \tag{21}$$

$$\Delta G = \Delta H^\circ - T\Delta S \tag{22}$$

The thermodynamic parameters (Table 7) demonstrate that the removal of Cu (II) and Cr (VI) ions from petroleum

Table 6. Kinetic models parameters for the adsorption of Cu (II) and Cr (VI) ions.

Selected heavy metals	Nano materials	Pseudo-first-order				Pseudo-second-order				Intraparticle diffusion				Elovich			
		R <sup>2</sup>	k <sub>1</sub> (mg/g·min)	q <sub>e1</sub> (g/min)	SSE	χ <sup>2</sup>	R <sup>2</sup>	k <sub>2</sub> (mg/g·min)	q <sub>e2</sub> (g/min)	SSE	χ <sup>2</sup>	R <sup>2</sup>	K <sub>id</sub> (g/min)	C	R <sup>2</sup>	β	α (g/m)
Cu (II)	ZnO	0.888	0.188	0.441	0.096	5.586	0.998	2.269	0.462	0.130	0.309	0.814	0.024	0.299	0.661	223.435	25.8
	Fe <sub>3</sub> O <sub>4</sub>	0.853	0.182	0.428	0.406	9.660	0.998	2.215	0.396	0.131	0.314	0.811	0.021	0.288	0.659	156.902	23.036
	ZnO/Fe <sub>3</sub> O <sub>4</sub>	0.898	0.196	0.464	0.064	2.462	0.999	2.447	0.49	0.063	0.161	0.918	0.027	0.343	0.898	459.164	34.698
Cr (VI)	ZnO	0.773	0.175	0.238	4.878	19.275	0.990	2.287	0.361	0.295	1.291	0.727	0.019	0.136	0.659	14.376	0.080
	Fe <sub>3</sub> O <sub>4</sub>	0.721	0.166	0.224	8.266	34.714	0.983	2.046	0.325	0.316	0.960	0.679	0.019	0.127	0.658	1.790	0.034
	ZnO/Fe <sub>3</sub> O <sub>4</sub>	0.886	0.193	0.305	4.635	15.205	0.993	2.726	0.426	0.266	0.978	0.821	0.028	0.191	0.819	69.102	0.134

refinery wastewater was endothermic, as evidenced by the positive values of standard enthalpy change ( $\Delta H^\circ$ ) at all temperatures. The Positive entropy values ( $\Delta S^\circ$ ) in Table 7 indicate a high affinity between the nanoadsorbent (ZnO, Fe<sub>3</sub>O<sub>4</sub> nanoparticles and ZnO/Fe<sub>3</sub>O<sub>4</sub> nanocomposite) and the heavy metals ions. This further implies that as the adsorption process increases, the adsorbent and adsorbate contact becomes more random.<sup>[70]</sup> The fact that ( $\Delta G^\circ$ ) values increase as temperature rises suggest that higher temperatures favor the adsorption process.<sup>[71]</sup> Cu (II) is more temperature-sensitive than Cr (VI), according to the results in Table 7 as evidenced by the lower value of ( $\Delta G^\circ$ ). This means that Cu (II) removal is more spontaneous than Cr (VI) due to the lower value of ( $\Delta G^\circ$ ).

### Comparison of selected heavy metals' percentage removal with previous studies

The results obtained in this study were compared with previous studies in the literature and the results are shown in Table 8

Table 8 shows that Cu (II) and Cr (VI) ions have a lower adsorptive removal efficiency on ZnO and Fe<sub>3</sub>O<sub>4</sub> nanoparticles compared to several other monometallic oxide nanoparticles reported in the literature. This could be a result of the authors using simulated wastewater, which contains fewer metal ions than actual industrial effluent. The presence of multiple contaminants in wastewater from a petroleum refinery may potentially be the cause of the poorer adsorption

**Table 7.** Thermodynamic parameters for the adsorption of Cu (II) and Cr (III) ions.

Selected heavy Metals	Nano materials	$\Delta G$ (kJ/mol)							
		$\Delta H \left( \frac{\text{kJ}}{\text{mol}} \right)$	$\Delta S \left( \frac{\text{J}}{\text{mol.K}} \right)$	303K	313K	323K	333K	343K	353K
Cu (II)	ZnO	10.015	16.451	5.030	4.866	4.701	4.537	4.372	4.208
	Fe <sub>3</sub> O <sub>4</sub>	8.521	11.913	4.911	4.792	4.673	4.554	4.435	4.316
	ZnO/Fe <sub>3</sub> O <sub>4</sub>	20.286	51.749	4.606	4.089	3.571	3.054	2.536	2.019
Cr (VI)	ZnO	33.000	37.875	21.524	21.145	20.766	20.388	20.009	19.630
	Fe <sub>3</sub> O <sub>4</sub>	36.000	33.000	26.001	25.671	25.341	25.011	24.681	24.351
	ZnO/Fe <sub>3</sub> O <sub>4</sub>	18.419	11.902	17.843	17.824	17.805	17.786	17.767	17.748

**Table 8.** Comparison of selected heavy metals percentage removal and other parameters on ZnO, Fe<sub>3</sub>O<sub>4</sub> nanoparticles and ZnO/Fe<sub>3</sub>O<sub>4</sub> nanocomposites.

Synthesis methods	Nanoadsorbent	Characterization tools	Crystallite size (nm)	Pollutants	Removal (%)	Other adsorption Conditions	References
Sol-gel	Fe <sub>3</sub> O <sub>4</sub>	TGA, SEM, XRD	56	Cr (VI)	72	pH (3), temperature (30 °C), adsorbent dosage (10 g) and contact time (110 min), concentration (10 mg/L)	[27]
Sol-gel	Fe <sub>3</sub> O <sub>4</sub>	SEM, XRD	13.38	Cr (VI),	72.45	Temperature (30 °C), contact time (4 h), pH of 2	[72]
Co-precipitation	Fe <sub>3</sub> O <sub>4</sub>	XRD, SEM, EDS, TEM,	12.3	Cu (II)	69.46	Adsorbent dosage of 0.05 g and 30 min of contacts time.	[20]
Precipitation	ZnO	FTI-R, SEM, FTI-R and TGA	73	Cu (II),	100, 77.47, 97.85	Stirred at 120 rpm at 150 min and adsorbent dosage of 0.1 g.	[73]
Co-precipitation	Fe <sub>3</sub> O <sub>4</sub>	SEM, XRD, FTI-R	27.68	Cr (VI)	80	pH (4), at room temperature, adsorbent dosage (25 mg/L), contact time (250 min)	[74]
Precipitation	ZnO	XRD, SEM and EDX	not available	Cr (VI)	98	pH of 3 at 40 min of contact time	[75]
Electrochemical	Fe <sub>3</sub> O <sub>4</sub>	TEM	12	Cr (VI)	100	pH (3.5) at room temperature, adsorbent dosage (2.5 g), contact time (2 h) concentration (25 mg/L)	[76]
Precipitation	Ultrafine mesoporous Fe <sub>3</sub> O <sub>4</sub>	BET, XRD, TEM		(II), Cu (II),	98, 87, 90, and 78	Adsorbent dosage (100 mg), pH of 1.0 at 25 °C using 50 mg L <sup>-1</sup> concentration of the water	[77]
Commercial nanoadsorbent	Fe <sub>3</sub> O <sub>4</sub>	SEM, XRD, FTI-R	20	Cr (VI), Cu (II)	88.83, 96.10	pH of 6, adsorbent dosage (2.5 g), contact time of 20 min at 45 °C	[78]
Co-precipitation	Fe <sub>3</sub> O <sub>4</sub> /talc	SEM, XRD, XPS	Not available	Cu (II),	72.15, 50.23, 91.35	Contact time of 25 min at 25 and adsorbent dosage of 0.12 g.	[79]
One-Pot	Amine/ Fe <sub>3</sub> O <sub>4</sub>	SEM, TEM, XRD, VSM	Not available	Cr (VI),	96 for both	pH of 6 and under 30 s at 298 °K	[80]
Co-precipitation	Rice straw/ Fe <sub>3</sub> O <sub>4</sub>	XRD, SEM, BET	Not available	Cu (II)	96.25, 75.54	Temperature (25 °C), adsorbent dosage (0.13 g) and contact time (41.96 and 59.35 s for Pb (II) and Cu (II), concentration 100 and 60 mg/L for Pb(II) and Cu(II)	[81]
Sol-gel- chemical reduction	Fe <sub>3</sub> O <sub>4</sub>	XRD, HRSEM FTI-R, EDX and BET	26.36	Cr (VI), Cu (II)	62.53, 80.57	Stirring speed of 250 rpm, nanoadsorbent dosage of 0.005 g and 15 min of Contact time at 35 °C	This work
Sol-gel	ZnO	XRD, HRSEM FTI-R, EDX and BET	20.12	Cr (VI), Cu (II)	65.19, 85.83	Stirring speed of 250 rpm, nanoadsorbent dosage of 0.005 g and 15 min of Contact time at 35 °C	This work
Sol-gel- chemical reduction	ZnO/ Fe <sub>3</sub> O <sub>4</sub>	XRD, HRSEM FTI-R, EDX and BET	14.50	Cr (VI), Cu (II)	77.60, 92.67	Stirring speed of 250 rpm, nanoadsorbent dosage of 0.005 g and 15 min of Contact time at 35 °C	



removal effectiveness compared to other previous research, which often competes with the pollutants for the active sites against using simulated wastewater which contains only the target heavy metal. The used experimental conditions may also be accountable for the variations in the adsorption removal of nanomaterials. For instance, in this study, the highest percentage of removal was within 15 min compared to the 30 minutes to 2 h reported in the literature. Additionally, the adsorbent dosage used in this study is 0.05 g compared to the 0.4 -10 g reported by the authors. The result from this study is better when compared with the analysis of<sup>[20]</sup> who used the same adsorbent dosage (0.05 g) under the applied condition of 30 min and reported a lower removal efficiency (69.46%) of Cu (II) ion compared to 85.43% reported in this study using ZnO and Fe<sub>3</sub>O<sub>4</sub> nanoparticles respectively. The lower adsorption efficiency may also be related to the crystallite size and synthesis method of the nanoparticles used for the elimination of the target pollutant.

The adsorption of Cr (VI) and Cu (II) ions onto ZnO/Fe<sub>3</sub>O<sub>4</sub> nanocomposites have comparable percentage adsorption removal to other bimetallic nanocomposites reported in Table 8. The result suggests that the size of the nanoparticles, morphology and method of synthesis had a significant impact on the adsorption process. Another possible explanation for the lower adsorption efficiency of the bimetallic oxides in this study may also be ascribed to the use of simulated wastewater by most of the authors which, when compared to actual industrial effluent, has a greater metal ion content.

#### Mechanisms of adsorption of the Cr (VI) and Cu (II) ions ZnO, Fe<sub>3</sub>O<sub>4</sub> nanoparticles and ZnO/Fe<sub>3</sub>O<sub>4</sub> nanocomposite

The adsorption of Cu (II) and Cr (VI) from petroleum refinery wastewater is greatly influenced by the PVP used as a capping and stabilizing agent during the synthesis of

nanoadsorbents. The PVP added onto the ZnO/Fe<sub>3</sub>O<sub>4</sub> nanocomposites donated electrons into the orbitals of the Zn and Fe ions while the nitrogen or carbonyl oxygen of the PVP repeating unit stabilizes the PVP/ZnO/Fe<sub>3</sub>O<sub>4</sub> nanocomposites (see Figure 9). This interaction resulted in the formation of both cation ions and anions groups that bind the heavy metals with both the nanoparticles and the nanocomposites via complexation, ion exchange, diffusion, Surface adsorption, transportation and precipitation mechanisms<sup>[82]</sup> (see Figure 10). This may either lead to physical adsorption or chemical adsorption

#### Leaching, desorption and reusability of the ZnO, Fe<sub>3</sub>O<sub>4</sub> nanoparticles and ZnO/Fe<sub>3</sub>O<sub>4</sub> nanocomposite

##### Desorption of the ZnO, Fe<sub>3</sub>O<sub>4</sub> nanoparticles and ZnO/Fe<sub>3</sub>O<sub>4</sub> nanocomposite

Various concentrations of HNO<sub>3</sub> (0.025, 0.08 and 0.1 moldm<sup>-3</sup>) were used as desorbing agents to examine the desorption characteristics of previously deposited Cu (II) and Cr (VI) on the surface of ZnO, Fe<sub>3</sub>O<sub>4</sub> nanoparticles and ZnO/Fe<sub>3</sub>O<sub>4</sub> nanocomposite and the result is presented in Figure 11.

Figure 11 depicts the effect of the different concentrations (0.025, 0.08 and 0.1 moldm<sup>-3</sup>) of HNO<sub>3</sub> as a desorbing agent. It can be seen that 0.100 moldm<sup>-3</sup> is a more effective desorbing agent for Cu (II) and Cr (VI), as it desorbs 81.83%, 80.86% and 90.80% of the adsorbed Cu (II) ions while 61.33%, 60.13% and 73.02%, of Cr (VI) ions desorbed from the surface of ZnO, Fe<sub>3</sub>O<sub>4</sub> nanoparticles and ZnO/Fe<sub>3</sub>O<sub>4</sub> nanocomposite respectively. This is because increasing the acid's concentration, the surface of ZnO, Fe<sub>3</sub>O<sub>4</sub> and ZnO/Fe<sub>3</sub>O<sub>4</sub> nanoadsorbents become more protonated and no longer attract positively charged metal ions, causing the protons to replace the bonded metal ions.

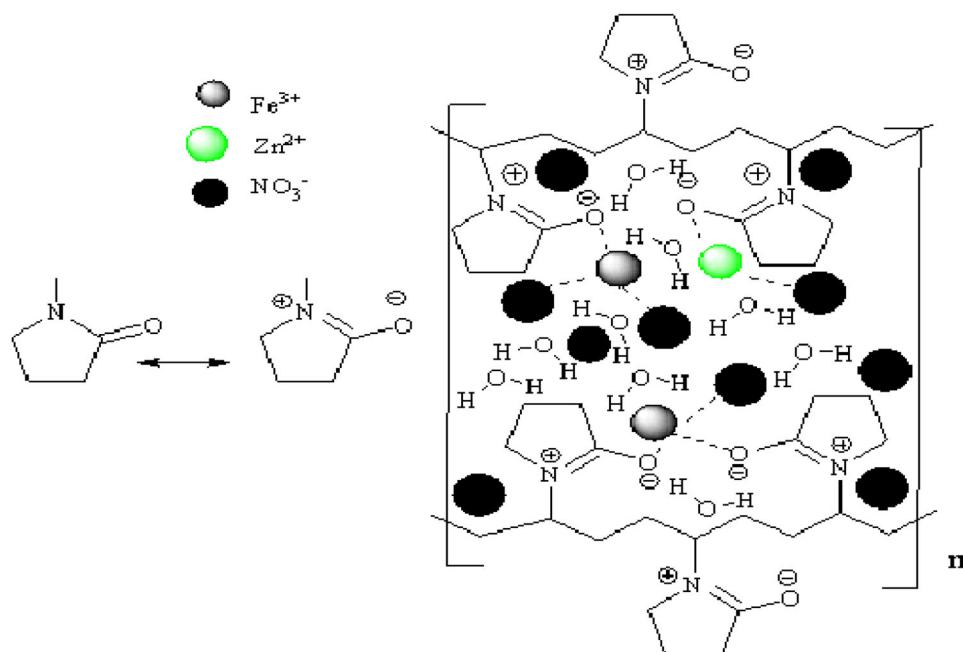


Figure 9. Interaction of PVP with Zn (II) and Fe (II) after the formation of the ZnO/Fe<sub>3</sub>O<sub>4</sub> nanocomposites.

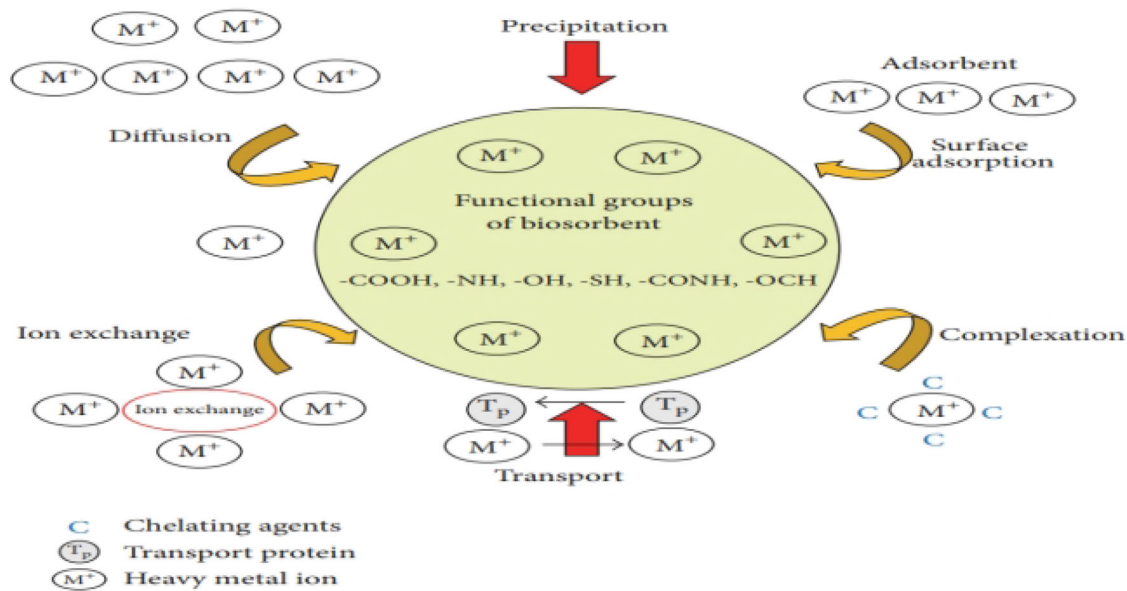


Figure 10. Adsorption mechanism for heavy metal removal.

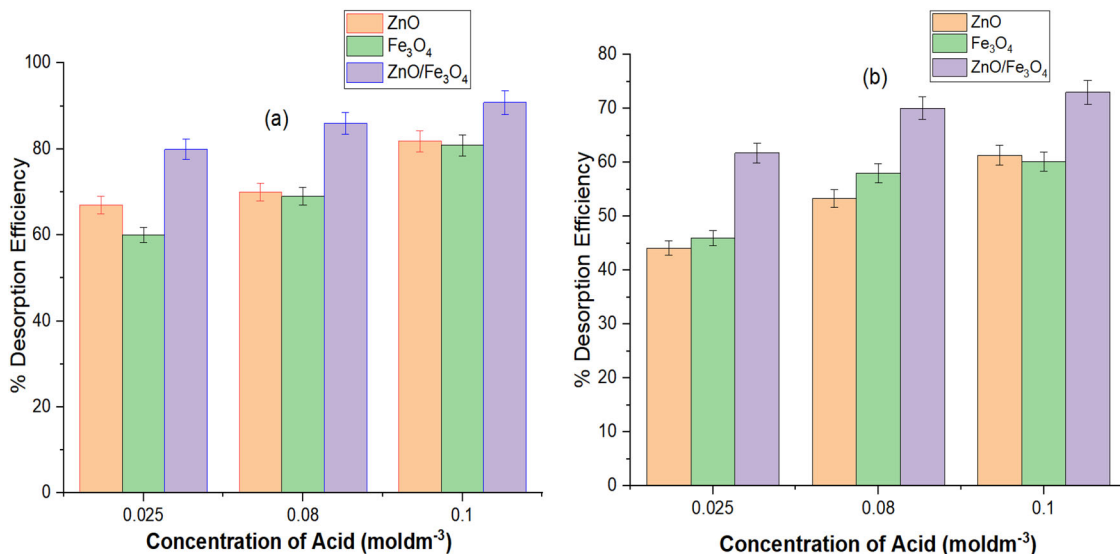


Figure 11. Percentage desorption of (a) Cu (II) and (b) Cr (VI) using different concentrations of nitric acid ( $HNO_3$ ) under the condition of adsorbent amount 0.25 g, pH = 6, desorption time (15 min), and reaction temperature ( $30^\circ C$ ).

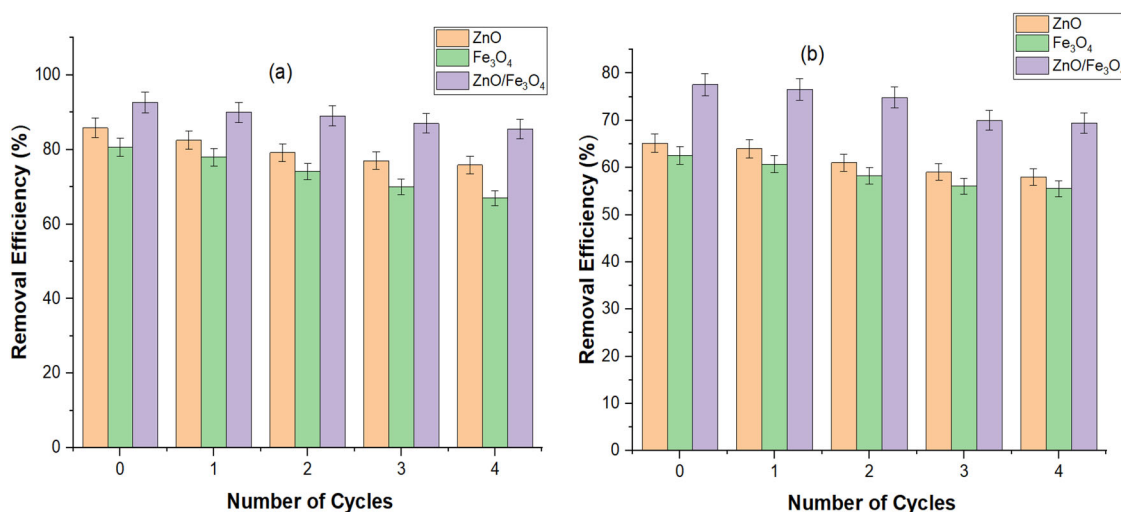
The high percentage desorption observed at a higher concentration of  $HNO_3$  suggested that Cu (II) and Cr (VI) ions were adsorbed onto both adsorbents by strong intermolecular forces via the chemisorption mechanism. The earlier result from the adsorption isotherm, kinetic, and thermodynamic analyses supported this data, that the adsorption of Cu (II) and Cr (VI) ions onto the surface of ZnO,  $Fe_3O_4$  and ZnO/ $Fe_3O_4$  nanoadsorbents is chemisorption. This result agrees with the conclusion<sup>[83]</sup> that poor desorption of metal ions from the nanoadsorbents surface may be caused by a lower concentration of the desorbing agents. However,<sup>[84]</sup> reported decreases in the desorption of Cu (II) as the concentration of acid increases. The differences observed may be linked to the type of adsorbent employed in this study.

#### Leaching of the ZnO, $Fe_3O_4$ nanoparticles and ZnO/ $Fe_3O_4$ nanocomposite

A leaching test was conducted on ZnO and  $Fe_3O_4$  nanoparticles and ZnO/ $Fe_3O_4$  nanocomposites used for the removal of Cu (II) and Cr (VI) ions from the petroleum refinery wastewater during the desorption studies. The leaching test was conducted at different concentrations (0.025, 0.08, 0.1 and  $0.2 \text{ mol dm}^{-3}$ ) of nitric acid ( $HNO_3$ ) solutions. This evaluation is important to determine the safety level of the nanoadsorbent. Table 9 shows that after 15 minutes of the desorption of ZnO,  $Fe_3O_4$  nanoparticles and ZnO/ $Fe_3O_4$  nanocomposites,  $0.099 \pm 0.11 \text{ mg/L}$  Fe ions were leached using  $0.025 \text{ mol dm}^{-3}$  of the nitric acid ( $HNO_3$ ) solution as a desorbing agent due to the none usage of any stabilizing or capping agent during the synthesis of the  $Fe_3O_4$

**Table 9.** Concentration of leached Metal ions in solution at a different acid concentration.

Nanoadsorbent	Concentration of the leachable ions (mg/L)	Concentration (mol dm <sup>-3</sup> )				WHO Permissible Limit (2017)
		0.025	0.08	0.1	0.2	
ZnO	Zn (mg/L)	ND	0.082 ± 0.02	0.103 ± 0.10	0.330 ± 0.11	5
Fe <sub>3</sub> O <sub>4</sub>	Fe (mg/L)	0.099 ± 0.11	0.102 ± 0.05	0.169 ± 0.02	0.383 ± 0.15	0.3
ZnO/Fe <sub>3</sub> O <sub>4</sub>	Zn (mg/L)	ND	ND	0.038 ± 0.02	0.126 ± 15	5
	Fe (mg/L)	ND	ND	0.095 ± 0.15	0.19 ± 11	0.3

**Figure 12.** Desorption-adsorbed of (a)Cu(II) and (b) Cr (VI) ion and reusability of ZnO, Fe<sub>3</sub>O<sub>4</sub> nanoparticles and ZnO/Fe<sub>3</sub>O<sub>4</sub> nanocomposites using 0.1 mol dm<sup>-3</sup> of HNO<sub>3</sub> acid as desorbing agent.

nanoparticles. At the same concentration of acid, Zn did not leach from ZnO. Similarly, both Fe and Zn ions were not leached at between 0.025 and 0.08 mol dm<sup>-3</sup> of the nitric acid (HNO<sub>3</sub>) solution as a desorbing agent due to the formation of a nanocomposite that is more stable than individual nanoparticles. As the concentration of the nitric acid (HNO<sub>3</sub>) solution increases from 0.08 to 0.2 mol dm<sup>-3</sup> there was leaching of both Zn (II) ions and Fe (II) ions for both the individual nanoparticles and the nanocomposites. The concentration of the metals leached into the solution falls well within the acceptable limit for various metal ions in drinking water except for Fe ions at at 0.2 mol dm<sup>-3</sup>[85]. Additionally, after the desorption of the heavy metals, the metal-rich aqueous phase was incorporated into concrete and the leaching test was carried out using 0.1 mol dm<sup>-3</sup>. The result indicates that the level of both the Cu (II) and Cr (VI) ions was less than the WHO permissible limit. Many researchers such as [86] have reported that the amounts of heavy metals (Cr, Ni, and Zn) in the bio-solids had no bearing on cement strength, initial setting time, or cement hydration. This method is an alternative method for the management of the waste generated from the adsorption process. Other researchers including [87,88] have reported other methods for managing spent sorbents and wastewater generated during the adsorption process including phytocapping and phytoremediation, which employ specific plant species.

#### Reusability of the ZnO, Fe<sub>3</sub>O<sub>4</sub> nanoparticles and ZnO/Fe<sub>3</sub>O<sub>4</sub> nanocomposite

Reusability studies aid in understanding the mechanisms of heavy metal removal and recovery from metal-loaded

adsorbents, as well as the reusability of the nanoadsorbents, which can save costs and help preserve the environment. The reusability of ZnO, Fe<sub>3</sub>O<sub>4</sub> and ZnO/Fe<sub>3</sub>O<sub>4</sub> nanoadsorbents were studied and the result is presented in Figure 12.

Figure 12 shows that the reusability efficiency of ZnO, Fe<sub>3</sub>O<sub>4</sub> nanoparticles and ZnO/Fe<sub>3</sub>O<sub>4</sub> nanocomposites were slightly reduced after each cycle (> 5%); nevertheless, in comparison to the initial use for Cu (II) (85.83%, 80.57% and 92.67%) and Cr (VI) (65.19%, 62.53% and 77.60%) by ZnO, Fe<sub>3</sub>O<sub>4</sub> and ZnO/Fe<sub>3</sub>O<sub>4</sub> nanocomposites, it retained its high adsorption potential. At the 4<sup>th</sup> cycle, the removal efficiencies were 75.84% 67.00%, 85.51 and 58.03%, 55.56%, 69.42% for Cu (II) and Cr (VI) using exhausted ZnO, Fe<sub>3</sub>O<sub>4</sub> and ZnO/Fe<sub>3</sub>O<sub>4</sub> nanoadsorbents respectively. This confirms that the ZnO, Fe<sub>3</sub>O<sub>4</sub> nanoparticles and ZnO/Fe<sub>3</sub>O<sub>4</sub> nanoadsorbent can be recycled after use, which lowers waste production and makes it a valuable application for the removal of heavy metal ions from wastewater. The findings of this study could be compared to other studies on desorption and reusability of exhausted adsorbents. For example, de-ionized water, pipe-borne water, 0.1 M H<sub>2</sub>SO<sub>4</sub>, 0.1 M HCl and 0.1 M NaOH were used as desorption agents for the desorption of chromium (VI) and lead (II) ions under the condition of desorption time (60 min) stirring speed (120 rpm) at 30 °C. The authors found that the acids were better desorbing agents for the heavy metals compared to de-ionized water, pipe-borne water and 0.1 M NaOH. The adsorption efficiency was maintained at 53.5% and 54.6% after the third cycle periods.[79] This result confirms the efficiency of acids compared to the other adsorbing agents used for the desorption of heavy metals.

## Conclusion

ZnO, Fe<sub>3</sub>O<sub>4</sub> nanoparticles and ZnO/Fe<sub>3</sub>O<sub>4</sub> nanocomposites were successfully synthesized via simple sol-gel chemical reduction methods which were confirmed by characterization techniques such as HRSEM, EDS, XRD, FTI-R and BET. The specific active surface area of ZnO and Fe<sub>3</sub>O<sub>4</sub> improved following the synthesis of ZnO/Fe<sub>3</sub>O<sub>4</sub> nanocomposites suggesting the existence of synergetic effects. The removal of Cu (II) and Cr (VI) ions from petroleum refinery wastewater was dependent on contact time, nano-adsorbent dosage and temperature. The adsorption processes indicate that the Langmuir model best fits the experimental data for both Cu (II) and Cr (VI) ions. The adsorption process shows that ZnO/Fe<sub>3</sub>O<sub>4</sub> nanocomposites was a better adsorbent for the removal of Cu (II) and Cr (VI) with percentage removal of 92.67% and 77.60%. The adsorption performance of all the adsorbents is best described by pseudo-second-order kinetic models, indicating that chemisorption reaction dominates the adsorption of Cu (II) and Cr (VI) ions by ZnO, Fe<sub>3</sub>O<sub>4</sub> nanoparticles and ZnO/Fe<sub>3</sub>O<sub>4</sub> composites. The adsorption of Cr (VI) was low for both ZnO, Fe<sub>3</sub>O<sub>4</sub> nanoparticles and ZnO/Fe<sub>3</sub>O<sub>4</sub> composites compared to Cu (II) ion at all the applied conditions. Different concentrations of HNO<sub>3</sub> (0.025, 0.08 and 0.1 moldm<sup>-3</sup>) solutions were used to desorb and recover ZnO, Fe<sub>3</sub>O<sub>4</sub> nanoparticles and ZnO/Fe<sub>3</sub>O<sub>4</sub> composites and it was discovered that 0.100 moldm<sup>-3</sup> is capable of desorbing 81.83%, 80.86% and 90.80% of Cu (II) ions; 61.33%, 60.13% and 73.02%, of Cr (VI) ions. It was also established that ZnO, Fe<sub>3</sub>O<sub>4</sub> nanoparticles and ZnO/Fe<sub>3</sub>O<sub>4</sub> composites still had a good ability for Cu (II) and Cr (VI) ions removal after four cycles. The result generally shows that ZnO/Fe<sub>3</sub>O<sub>4</sub> composites exhibited better performance than the individual nanoparticles and thus serve as a potential adsorbent for the adsorption of Cu (II) and Cr (VI) ions from petroleum refinery wastewater.

## Acknowledgments

The authors appreciate the contribution of the following people for their technical assistance: Dr. Remy Bucher (XRD analysis, iThemba Labs, South Africa); Dr. Franscious Cummings (HRSEM/HRTEM/SAED/EDS) analysis, Physics department, University of the Western Cape (UWC), South Africa); and Prof. W.D. Roos for XPS analysis. Mr. Sandeeran Govender (BET analysis), Chemical Engineering Department, University of Cape Town, South Africa.

## Declaration of competing interest

There are no conflicts to declare

## ORCID

E. Y. Shaba  <http://orcid.org/0000-0001-5240-091X>

## Data availability statement

The authors confirm that the data supporting the findings of this study are available within the article.

## Funding

The author(s) reported there is no funding associated with the work featured in this article.

## References

- [1] Kılıç, Z. The Importance of Water and Conscious Use of Water. *IJH* **2020**, *4*, 239–241. DOI: [10.15406/ijh.2020.04.00250](https://doi.org/10.15406/ijh.2020.04.00250).
- [2] Falinski, M. M.; Turley, R. S.; Kidd, J.; Lounsbury, A. W.; Lanzarini-Lopes, M.; Backhaus, A.; Rudel, H. E.; Lane, M. K. M.; Fausey, C. L.; Barrios, A. C.; et al. Doing Nano-Enabled Water Treatment Right: sustainability Considerations from Design and Research through Development and Implementation. *Environ. Sci.: Nano* **2020**, *11*, 1–24.
- [3] WHO. 2021. Protection of the Human Environment. <https://www.afro.who.int/health-topics/water> (accessed Jun 27, 2022).
- [4] Ohanmu, E. O.; Bako, S. P.; Ohanmu, E.; Ohanmu, O. O. Environmental Implications, Properties and Attributes of Crude Oil in the Oil-Producing States of Nigeria. *Ecologi* **2018**, *9*, 1–9. DOI: [10.3923/ecologia.2019.1.9](https://doi.org/10.3923/ecologia.2019.1.9).
- [5] Khatoun, K.; Malik, A. Cyto-Genotoxic Potential of Petroleum Refinery Wastewater Mixed with Domestic Sewage Used for Irrigation of Food Crops in the Vicinity of an Oil Refinery. *Heliyon* **2021**, *7*, e08116–15. DOI: [10.1016/j.heliyon.2021.e08116](https://doi.org/10.1016/j.heliyon.2021.e08116).
- [6] Adeola, A. O.; Akingboye, A. S.; Ore, O. T.; Oluwajana, O. A.; Adewole, A. H.; Olawade, A. D. B.; Ogunyele, A. C. Crude Oil Exploration in Africa: socio-Economic Implications, Environmental Impacts, and Mitigation Strategies. *Environ. Syst. Decis.* **2022**, *42*, 26–50.
- [7] Makeen, Y. M.; Shan, X.; Lawal, M.; Ayinla, H. A.; Su, S.; Yelwa, N. A.; Liang, Y.; Ayuk, N. E.; Du, X. Reservoir Quality and Its Controlling Diagenetic Factors in the Bentiu Formation, Northeastern Muglad Basin, Sudan. *Sci. Rep.* **2021**, *11*, 1–13. DOI: [10.1038/s41598-021-97994-x](https://doi.org/10.1038/s41598-021-97994-x).
- [8] Briffa, J.; Sinagra, E.; Blundell, R. Heavy Metal Pollution in the Environment and Their Toxicological Effects on Humans. *Heliyon* **2020**, *6*, e04691–20. DOI: [10.1016/j.heliyon.2020.e04691](https://doi.org/10.1016/j.heliyon.2020.e04691).
- [9] Moharbi, S. S.; Geetha, M.; Devi, B. M.; Sangeetha, S. J. Studies on the Removal of Copper Ions from Industrial Effluent by Azadirachta Indica Powder. *Appl. Water Sci.* **2020**, *10*, 1–10. DOI: [10.1007/s13201-019-1100-z](https://doi.org/10.1007/s13201-019-1100-z).
- [10] Engwa, G. A.; Ferdinand, P. U.; Nwalo, F. N.; Unachukwu, M. N. Mechanism and Health Effects of Heavy Metal Toxicity in Humans. In *Poisoning in the Modern World - New Tricks for an Old Dog?*; Karcioğlu, O., Arslan, B., Eds.; Intech Open: London, UK, **2019**. DOI: [10.5772/intechopen.82511](https://doi.org/10.5772/intechopen.82511).
- [11] Balali-Mood, M.; Naseri, K.; Tahergorabi, Z.; Khazdair, M. R.; Sadeghi, M. Toxic Mechanisms of Five Heavy Metals: mercury Lead Chromium Cadmium and Arsenic. *Front. Pharmacol.* **2021**, *12*, 1–19. DOI: [10.3389/fphar.2021.643972](https://doi.org/10.3389/fphar.2021.643972).
- [12] Narayanan, C. M.; Narayan, V. Biological Wastewater Treatment and Bioreactor Design: A Review. *Sustain. Environ. Res.* **2019**, *29*, 1–17. DOI: [10.1186/s42834-019-0036-1](https://doi.org/10.1186/s42834-019-0036-1).
- [13] Li, M.; Hu, K.; Wang, J. Study on Optimal Conditions of Flocculation in Drinking Wastewater Treatment. *J. Eng. Appl. Sci.* **2021**, *35*, 1–14.
- [14] Qasem, N. A. A.; Mohammed, R. H.; Lawal, D. U. Removal of Heavy Metal Ions from Wastewater: A Comprehensive and Critical Review. *Npj Clean Water* **2021**, *4*, 1–15. DOI: [10.1038/s41545-021-00127-0](https://doi.org/10.1038/s41545-021-00127-0).
- [15] Zhao, Q.; Xu, T.; Song, X.; Nie, S.; Choi, S. E.; Chuanling, S. I. Preparation and Application in Water Treatment of Magnetic Biochar. *Front. Bioeng. Biotechnol.* **2021**, *9*, 2296–4185.
- [16] Kumar, J.; Joshi, H.; Malyan, S. K. Removal of Copper, Nickel, and Zinc Ions from an Aqueous Solution through Electrochemical and Nanofiltration Membrane Processes. *Appl. Sci.* **2022**, *12*, 1–15.



- [17] El-Batouti, M.; Al-Harby, N. F.; Elewa, M. M. A. Review on Promising Membrane Technology Approaches for Heavy Metal Removal from Water and Wastewater to Solve Water Crisis. *Water* **2021**, *13*, 3241–3262. DOI: [10.3390/w13223241](https://doi.org/10.3390/w13223241).
- [18] Hussain, S. T.; Ali, S. A. K. Removal of Heavy Metal by Ion Exchange Using Bentonite Clay. *J. Ecol. Eng.* **2021**, *22*, 104–111. DOI: [10.12911/22998993/128865](https://doi.org/10.12911/22998993/128865).
- [19] Sylwan, I.; Thorin, E. Removal of Heavy Metals during Primary Treatment of Municipal Wastewater and Possibilities of Enhanced Removal: A Review. *Water* **2021**, *13*, 1121. DOI: [10.3390/w13081121](https://doi.org/10.3390/w13081121).
- [20] Iconaru, S. L.; Guégan, R.; Popa, C. L.; Motelica-Heino, M.; Ciobanu, C. S.; Predoi, D. Magnetite (Fe<sub>3</sub>O<sub>4</sub>) Nanoparticles as Adsorbents for as and Cu Removal. *Appl. Clay Sci.* **2016**, *134*, 128–135. DOI: [10.1016/j.clay.2016.08.019](https://doi.org/10.1016/j.clay.2016.08.019).
- [21] Crini, G.; Lichtfouse, E.; Wilson, L. D.; Morin-Crini, N. Conventional and Non-Conventional Adsorbents for Wastewater Treatment. *Environ. Chem. Lett.* **2018**, *17*, 1–19.
- [22] Shaba, E. Y.; Jacob, J. O.; Tijani, J. O.; Suleiman, M. A. T. A Critical Review of Synthesis Parameters Affecting the Properties of Zinc Oxide Nanoparticle and Its Application in Wastewater Treatment. *Appl. Water Sci.* **2021**, *11*, 1–48. DOI: [10.1007/s13201-021-01370-z](https://doi.org/10.1007/s13201-021-01370-z).
- [23] Hezami, L.; Modwi, A.; Ghiloufi, I.; Taha, K. K.; Bououdina, M.; ElJery, A.; El, L.; Mir, L. Effect of Aluminum Loading on Structural and Morphological Characteristics of ZnO Nanoparticles for Heavy Metal Ion Elimination. *Environ. Sci. Pollut. Res.* **2020**, *27*, 3086–3099. DOI: [10.1007/s11356-019-07279-0](https://doi.org/10.1007/s11356-019-07279-0).
- [24] Dhiman, V.; Kondal, N. ZnO Nano-adsorbents: A Potent Material for Removal of Heavy Metal Ions from Wastewater. *Colloid Interface Sci. Commun.* **2021**, *14*, 1–26.
- [25] Leiva, E.; Tapia, C.; Rodríguez, C. Highly Efficient Removal of Cu(II) Ions from Acidic Aqueous Solution Using ZnO Nanoparticles as nano-Adsorbents. *Water* **2021**, *13*, 2960. DOI: [10.3390/w13212960](https://doi.org/10.3390/w13212960).
- [26] Stoian, O.; Covaliu, C. I.; Paraschiv, G.; Catrina, G. A.; Nit, M. E.; Matei, S. S.; Biri, S. S.; Tudor, P. Magnetite Oxide Nanomaterial Used for Lead Ions Removal from Industrial Wastewater. *Materials* **2021**, *14*, 1–11.
- [27] Padmavathy, K. M.; Madhu, G.; Haseena, P. A. A. Study on the Effects of Ph, Adsorbent Dosage, Time, Initial Concentration and Adsorption Isotherm Study for the Removal of Hexavalent Chromium (Cr (IV)) from Wastewater by Magnetite Nanoparticles. *Procedia Technol.* **2016**, *24*, 585–594. DOI: [10.1016/j.protcy.2016.05.127](https://doi.org/10.1016/j.protcy.2016.05.127).
- [28] Zhao, C.; Wang, X.; Zhang, S.; Sun, N.; Zhou, H.; Wang, G.; Zhao, H. Porous Carbon Nanosheets Functionalized with Fe<sub>3</sub>O<sub>4</sub> Nanoparticles for Capacitive Removal of Heavy Metal Ions from Water. *Environ. Sci.: Water Res. Technol.* **2020**, *6*, 331–340.
- [29] Aguilar-Pérez, K. M.; Avilés-Castrillo, J. I.; Ruiz-Pulido, G.; Medina, D. I.; Parra-Saldivar, R.; Iqbal, H. M. N. Nano-adsorbents in Focus for the Remediation of Environmentally-Related Contaminants with Rising Toxicity Concerns. *Sci. Total Environ.* **2021**, *779*, 146465. DOI: [10.1016/j.scitotenv.2021.146465](https://doi.org/10.1016/j.scitotenv.2021.146465).
- [30] Ganapathe, L. S.; Mohamed, M. A.; Mohamad, Y.; Rozan, B.; Dilla, D. Magnetite (Fe<sub>3</sub>O<sub>4</sub>) Nanoparticles in Biomedical Application: From Synthesis to Surface Functionalisation. *Magnetochemistry* **2020**, *6*, 68. DOI: [10.3390/magnetochemistry6040068](https://doi.org/10.3390/magnetochemistry6040068).
- [31] Raka, M.; Sirshendu, D. Removal of Copper (II) from Aqueous Solution Using Zinc Oxide Nanoparticle Impregnated Mixed Matrix Hollow Fiber Membrane. *Environ. Technol. Innov.* **2022**, *26*, 1–21.
- [32] Natrayan, L.; Rajalakshmi, R.; Singh, K. A.; Patil, P. P.; Veeman, D.; Paramasivam, P. Synthesis and Optimization of Cr (VI) Removal from Aqueous Solution by Activated Carbon with Magnetic Fe<sub>3</sub>O<sub>4</sub> Nanoparticles by Response Surface Methodology. *Adsorp. Sci. Technol.* **2022**, *2022*, 1–9. DOI: [10.1155/2022/9366899](https://doi.org/10.1155/2022/9366899).
- [33] Gómez-Aguilar, D. L.; Esteban-Muñoz, J. A.; Rodríguez-Miranda, J. P.; Baracaldo-Guzmán, D.; Salcedo-Parra, O. J. Desorption of Coffee Pulp Used as an Adsorbent Material for Cr(III and VI) Ions in Synthetic Wastewater: A Preliminary Study. *Molecules* **2022**, *27*, 2170 1–16. DOI: [10.3390/molecules27072170](https://doi.org/10.3390/molecules27072170).
- [34] Farahmandjou, M.; Soflaee, F. Synthesis of Iron Oxide Nanoparticles Using Borohydride Reduction. *Int. J. Bio-Inorg. Nanomater.* **2015**, *3*, 203–206.
- [35] Kumaresan, N.; Ramamurthi, K. Synthesis of ZnO/rGO Nanocomposites by Wet Impregnation Method for Photocatalytic Performance against RHB Dye and 4-Chlorophenol under UV Light Irradiation. *J. Mater. Sci. Mater. Electron.* **2022**, *31*, 30–39.
- [36] Edokpayi, O.; Osemwenkhae, O.; Ayodele, B. V.; Ossai, J.; Fadilat, S. A.; Ogbeide, S. E. Batch Adsorption Study of Methylene Blue in Aqueous Solution Using Activated Carbons from Rice Husk and Coconut Shell. *J. Appl. Sci. Environ. Manage.* **2018**, *22*, 631–635.
- [37] Shaba, E. Y.; Tijani, J. O.; Jacob, J. O.; Suleiman, M. A. T. Adsorptive Potential of ZnO/SiO<sub>2</sub> Nanorods Prepared via the Sol-Gel Method for the Removal of Pb(II) and Cd(II) from Petroleum Refinery Wastewater. *J. Chem. Technol. Biotechnol.* **2022**, *8*, 1–22.
- [38] Kalam, S.; Abu-Khamsin, S. A.; Kamal, M. S.; Patil, S. Surfactant Adsorption Isotherms: A Review. *Am. Chem. Soc.* **2021**, *6*, 32342–32348.
- [39] Sharif, F.; Roberts, E. P. L. Electrochemical Oxidation of an Organic Dye Adsorbed on Tin Oxide and Antimony Doped Tin Oxide Graphene Composites. *Catalysts* **2020**, *10*, 263. DOI: [10.3390/catal10020263](https://doi.org/10.3390/catal10020263).
- [40] Haixi, T.; Li, H.; Lin, M.; Kegang, L. Preparation of a Pinosresinol Diglucoside Imprinted Polymer Using Metal Organic Frame as the Matrix for Extracting Target Compound from *Eucommia Ulmoides*. *Sep. Sci. Technol.* **2021**, *15*, 1–5.
- [41] Jasper, F. E.; Ajibola, V. O.; Onwuka, J. C. Nonlinear Regression Analysis of the Sorption of Crystal Violet and Methylene Blue from Aqueous Solutions onto an Agro-Waste Derived Activated Carbon. *Appl. Water Sci.* **2020**, *10*, 1–11. DOI: [10.1007/s13201-020-01218-y](https://doi.org/10.1007/s13201-020-01218-y).
- [42] Pholosi, A.; Naidoo, E. B.; Ofomaja, A. E. Intraparticle Diffusion of Cr (VI) through Biomass and Magnetite Coated Biomass: A Comparative Kinetic and Diffusion Study. *South Af. J. Chem. Eng.* **2020**, *32*, 39–55. DOI: [10.1016/j.sajce.2020.01.005](https://doi.org/10.1016/j.sajce.2020.01.005).
- [43] Adeogun, A. I.; Balakrishnan, R. B. Kinetics Isothermal and Thermodynamics Studies of Electrocoagulation Removal of Basic Dye Rhodamine B from Aqueous Solution Using Steel Electrodes. *Appl. Water Sci.* **2017**, *7*, 1711–1723. DOI: [10.1007/s13201-015-0337-4](https://doi.org/10.1007/s13201-015-0337-4).
- [44] Shrestha, B.; Wang, L.; Zhang, H.; Hung, C. Y.; Tang, L. Gold Nanoparticles Mediated Drug-Gene Combinational Therapy for Breast Cancer Treatment. *IJN* **2020**, *ume 15*, 8109–8119. DOI: [10.2147/IJN.S258625](https://doi.org/10.2147/IJN.S258625).
- [45] Araújo, J.; Edgar, A.; Nobre, F. X.; Sousa, G. S.; Cavalcante, L. S.; Rita, M. S.; Souza, F. L.; Elias, M. J. M. Synthesis, Growth Mechanism, Optical Properties and Catalytic Activity of ZnO Microcrystals Obtained via Hydrothermal Processing. *RSC Adv.* **2017**, *7*, 24263–24281. DOI: [10.1039/C7RA03277C](https://doi.org/10.1039/C7RA03277C).
- [46] Diallo, A.; Ngom, B. D.; Park, E.; Maaza, M. Green Synthesis of ZnO Nanoparticles by *Aspalathus Linearis*: Structural & Optical Properties. *J. Alloys Compd.* **2015**, *646*, 425–430. DOI: [10.1016/j.jallcom.2015.05.242](https://doi.org/10.1016/j.jallcom.2015.05.242).
- [47] Ruiz-Baltazar, A.; Esparza, R.; Rosas, G.; Pérez, R. Effect of the Surfactant on the Growth and Oxidation of Iron Nanoparticles. *J. Nanomater.* **2015**, *2015*, 1–8. DOI: [10.1155/2015/240948](https://doi.org/10.1155/2015/240948).
- [48] Abdelhamid, H. N.; Wu, H. F. Multifunctional Graphene Magnetic Nanosheet Decorated with Chitosan for Highly Sensitive Detection of Pathogenic Bacteria. *J Mater. Chem. B* **2013**, *1*, 3950–3961. DOI: [10.1039/c3tb20413h](https://doi.org/10.1039/c3tb20413h).
- [49] Gopal, J.; Abdelhamid, H. N.; Hua, P.-Y.; Wu, H. F. Chitosan Nanomagnets for Effective Extraction and Sensitive Mass

- Spectrometric Detection of Pathogenic Bacterial Endotoxin from Human Urine. *J. Mater. Chem. B* **2013**, *1*, 2463–2475. DOI: [10.1039/c3tb20079e](https://doi.org/10.1039/c3tb20079e).
- [50] Ulya, N. H.; Taufiq, A. S. Comparative Structural Properties of Nanosized ZnO/Fe<sub>3</sub>O<sub>4</sub> Composites Prepared by Sonochemical and Sol-Gel Methods. *IOP Conf. Ser.: Earth Environ. Sci.* **2019**, *276*, 1–10.
- [51] Długosz, O.; Szostak, K.; Krupiński, M.; Banach, M. Synthesis of Fe<sub>3</sub>O<sub>4</sub>/ZnO Nanoparticles and Their Application for the Photodegradation of Anionic and Cationic Dyes. *Int. J. Environ. Sci. Technol.* **2021**, *18*, 561–574. DOI: [10.1007/s13762-020-02852-4](https://doi.org/10.1007/s13762-020-02852-4).
- [52] Abdolmohammad-Zadeh, H.; Zamani, A.; Shamsi, Z. A Simple Magnetic Solid-Phase Extraction Method Based on Magnetite/Graphene Oxide Nanocomposite for Pre-Concentration and Determination of Melamine by High-Performance Liquid Chromatography. *Environ. Sci. Pollut. Res.* **2020**, *27*, 1–9.
- [53] Singh, P. K.; Gautam, A.; Verma, V.; Singh, P. M.; Shivapriya, S.; Shivalkar, A. K.; Sahoo, S.; Kumar, A. Green Synthesis of Metallic Nanoparticles as Effective Alternatives to Treat Antibiotics Resistant Bacterial Infections: A Review. *Biotechnol. Rep.* **2020**, *25*, 1–11.
- [54] Singh, H.; Kumar, A.; Thakur, A.; Kumar, P.; Nguyen, V.-H.; Vo, D.-V. N.; Sharma, A.; Kumar, D. One-Pot Synthesis of magnetite-ZnO Nanocomposite and Its Photocatalytic Activity. *Top. Catal.* **2020**, *63*, 1097–1108.
- [55] Verbraeken, M. C.; Brandani, S. A Priori Predictions of Type I and Type V Isotherms by the Rigid Adsorbent Lattice Fluid. *Adsorption* **2020**, *26*, 989–1000. DOI: [10.1007/s10450-019-00174-7](https://doi.org/10.1007/s10450-019-00174-7).
- [56] Aljameel, A. I.; Ali, M. K. Zinc Oxide Thin Films Preparation by Chemical Methods onto Si Substrate for Solar Cell Application. *J. Non-Oxide Glas.* **2021**, *13*, 21–29.
- [57] Marcos-Hernández, M.; Villagrán, D. Mesoporous Composite Nanomaterials for Dye Removal and Other Applications. *Compos. Nanoadsorbents*, Elsevier, Amsterdam, Netherlands, **2019**, 265–293.
- [58] Li, X.; He, S.; Feng, C.; Zhu, Y.; Pang, Y.; Hou, J. Non-Competitive and Competitive Adsorption of Pb (II) and Zn (II) Ions onto SDS in Process of Micellar-Enhanced Ultrafiltration. *Sustainability* **2018**, *1*, 1–12.
- [59] Gebretsadik, H.; Gebrekidan, A.; Demlie, L. Removal of Heavy Metals from Aqueous Solutions Using EucalyptusCamaldulensis: An Alternate Low-Cost Adsorbent. *Cogent. Chem.* **2020**, *6*, 25–32.
- [60] Mouni, L.; Belkhir, L.; Bollinger, J.-C.; Bouzaza, A.; Assadi, A.; Tirri, A.; Dahmoune, F.; Madani, K.; Remini, H. Removal of Methylene Blue from Aqueous Solutions by Adsorption on Kaolin: kinetic and Equilibrium Studies. *Appl. Clay Sci.* **2018**, *153*, 38–45. DOI: [10.1016/j.clay.2017.11.034](https://doi.org/10.1016/j.clay.2017.11.034).
- [61] Edet, U. A.; Ifealebuegu, A. O. Kinetics Isotherms and Thermodynamic Modeling of the Adsorption of Phosphates from Model Wastewater Using Recycled Brick Waste. *Processes* **2020**, *8*, 665. DOI: [10.3390/pr8060665](https://doi.org/10.3390/pr8060665).
- [62] Xu, P.; Zeng, G. M.; Huang, D. L.; Yan, M.; Chen, M.; Lai, C.; Jiang, H.; Wu, H. P.; Chen, G. M.; Wan, J. Fabrication of Reduced Glutathione Functionalized Iron Oxide Nanoparticles for Magnetic Removal of Pb (II) from Wastewater. *J. Taiwan Inst. Chem. Eng.* **2017**, *71*, 165–173. DOI: [10.1016/j.jtice.2016.11.031](https://doi.org/10.1016/j.jtice.2016.11.031).
- [63] Fan, X.; Liu, H.; Anang, E.; Ren, D. Effects of Electronegativity and Hydration Energy on the Selective Adsorption of Heavy Metal Ions by Synthetic NaX Zeolite. *Materials (Basel)* **2021**, *14*, 4066. DOI: [10.3390/ma14154066](https://doi.org/10.3390/ma14154066).
- [64] Bankole, M. T.; Abdulkareem, A. S.; Tijani, J. O.; Ochigbo, S. S.; Afolabi, A. S.; Roos, W. D. Chemical Oxygen Demand Removal from Electroplating Wastewater by Purified and Polymer Functionalized Carbon Nanotubes Adsorbents. *Water Resour. Ind.* **2017**, *18*, 33–50. DOI: [10.1016/j.wri.2017.07.001](https://doi.org/10.1016/j.wri.2017.07.001).
- [65] Ramadoss, R.; Subramaniam, D. Removal of Divalent Nickel from Aqueous Solution Using Blue-Green Marine Algae: adsorption Modeling and Applicability of Various Isotherm Models. *Sep. Sci. Technol.* **2018**, *54*, 1–19.
- [66] Lshabanat, M.; Al-Mufarj, R. S.; Al-Senani, G. M. Study on Adsorption of Malachite Green by Date Palm Fiber. *Orient. J. Chem.* **2016**, *32*, 3139–3144. DOI: [10.13005/ojc/320636](https://doi.org/10.13005/ojc/320636).
- [67] Singh, S.; Anil, A. G.; Khasnabis, S.; Kumar, V.; Nath, B.; Adiga, V.; Kumar Naik, T. S.; Subramanian, S.; Kumar, V.; Singh, J.; Ramamurthy, P. C. Sustainable Removal of Cr (VI) Using Graphene Oxide-Zinc Oxide Nano: Adsorption Kinetics, Isotherms and Thermodynamics. *Environ. Res.* **2022**, *203*, 111891. DOI: [10.1016/j.envres.2021.111891](https://doi.org/10.1016/j.envres.2021.111891).
- [68] Manjuladevi, M.; Anitha, R.; Manonmani, S. Kinetic Study on Adsorption of Cr (VI), Ni (II), Cd (II) and Pb (II) Ions from Aqueous Solutions Using Activated Carbon Prepared from Cucumis Melo Peel. *Appl. Water Sci.* **2018**, *8*, 1–8.
- [69] Zand, A. D.; Abyaneh, M. R. Adsorption of Lead, Manganese, and Copper onto Biochar in Landfill Leachate: implication of Non-Linear Regression Analysis. *Sustain. Environ. Res.* **2020**, *30*, 1–13. DOI: [10.1186/s42834-020-00061-9](https://doi.org/10.1186/s42834-020-00061-9).
- [70] Ahmad, K. S.; Jaffri, S. B. Phytosynthetic Ag Doped ZnO Nanoparticles: Semiconducting Green Remediators: Photocatalytic and Antimicrobial Potential of Green Nanoparticles. *Open Chem.* **2018**, *16*, 556–570. DOI: [10.1515/chem-2018-0060](https://doi.org/10.1515/chem-2018-0060).
- [71] Amadi, O. K.; Okoro, I. A.; Uko, A. E. Isotherm and Thermodynamic Studies on Biosorption of Metal (ii) Ions from Aqueous Solution Using Calopogonium Muconoides (Calopo) Seed Pod. *ChemSearch J* **2021**, *12*, 31–40.
- [72] Agarwal, M.; Dey, P.; Upadhayaya, S.; Dohare, R. Adsorption Efficiency of Magnetite Nanoparticles for Chromium (VI) Removal from Water. *J. Indian Chem. Soc.* **2016**, *93*, 199–209.
- [73] Anusa, R.; Ravichandran, C.; Sivakumar, E. K. T. Removal of Heavy Metal Ions from Industrial Waste Water by nano-ZnO in Presence of Lectrogeneratedenton's Reagent. *Int. J. ChemTech Res.* **2017**, *10*(7), 501–508.
- [74] Hossain, M. T.; Hossain, M. M.; Begum, M. H. A.; Shahjahan, M.; Islam, M. M.; Saha, B. Magnetite (Fe<sub>3</sub>O<sub>4</sub>) Nanoparticles for Chromium Removal. *Bangladesh J. Sci. Ind. Res.* **2018**, *53*, 219–224. DOI: [10.3329/bjsir.v53i3.38269](https://doi.org/10.3329/bjsir.v53i3.38269).
- [75] Kamath, S.; Gopal, V.; Ramanjaneyalu, V.; Kamila, S. Application of ZnO Nano Rods for the Batch Adsorption of Cr (VI): a Study of Kinetics and Isotherms. *Am. J. Appl. Sci.* **2019**, *16*, 1–12.
- [76] Rivera, F. L.; Palomares, F. J. H.; Pilar, M. E. Improvement in Heavy Metal Removal from Wastewater Using an External Magnetic Inductor. *Nanomater* **2019**, *9*, 1–15.
- [77] Fato, F. P.; Li, D. Z.; Zhao, L.; Qiu, K.; Long, Y. Simultaneous Removal of Multiple Heavy Metal Ions from River Water Using Ultrafine Mesop Magnetite Nanoparticles. *ACS Omega* **2019**, *4*, 7543–7549. DOI: [10.1021/acsomega.9b00731](https://doi.org/10.1021/acsomega.9b00731).
- [78] Zhang, M.; Yin, Q.; Ji, X.; Wang, F.; Gao, X.; Zhao, M. High and Fast Adsorption of Cd (II) and Pb(II) Ions from Aqueous Solutions by a Waste Biomass Based Hydrogel. *Sci. Rep.* **2020**, *10*, 1–13. DOI: [10.1038/s41598-020-60160-w](https://doi.org/10.1038/s41598-020-60160-w).
- [79] Kalantari, K.; Ahmad, M. B.; Masoumi, H. R.; Shameli, K.; Basri, K.; Khandanlou, R. Rapid Adsorption of Heavy Metals by Fe<sub>3</sub>O<sub>4</sub>/Talc Nanocomposite and Optimization Study Using Response Surface Methodology. *Int. J. Mol. Sci.* **2014**, *15*, 1–27.
- [80] Norouzian, B. A.; Mahvi, A. H.; Gholami, M.; Rastkari, N.; Delikhooon, M. One-Pot Synthesis, Characterization and Adsorption Studies of Amine-Functionalized Magnetite Nanoparticles for Removal of Cr (VI) and Ni (II) Ions from Aqueous Solution: kinetic, Isotherm and Thermodynamic Studies. *J. Environ. Health Sci. Eng.* **2016**, *14*, 1–12.
- [81] Khandanlou, R.; Ahmad, M. B.; Fard Masoumi, H. R.; Shameli, K.; Basri, M.; Kalantari, K. Rapid Adsorption of Copper (II) and Lead (II) by Rice Straw/Fe<sub>3</sub>O<sub>4</sub> Nanocomposite: Optimization, Equilibrium Isotherms, and Adsorption Kinetics Study. *PLoS One.* **2015**, *10*, e0120264-19. DOI: [10.1371/journal.pone.0120264](https://doi.org/10.1371/journal.pone.0120264).
- [82] Nasser-Abdelhamid, H.; Mathew, A. P. Cellulose-Zeolitic Imidazolate Frameworks (CelloZIFs) for Multifunctional

- Environmental Remediation: Adsorption and Catalytic Degradation. *Chem. Eng. J.* **2021**, *426*, 131733. DOI: [10.1016/j.cej.2021.131733](https://doi.org/10.1016/j.cej.2021.131733).
- [83] Liu, H.; Zhang, H.; Wang, J.; Wei, J. Effect of Temperature on the Size of Biosynthesized Silver Nanoparticle: Deep Insight into Microscopic Kinetics Analysis. *Arab. J. Chem.* **2020**, *13*, 1011–1019. DOI: [10.1016/j.arabjc.2017.09.004](https://doi.org/10.1016/j.arabjc.2017.09.004).
- [84] Bayuo, J.; Abukari, M. A.; Pelig-Ba, K. B. Desorption of Chromium (VI) and Lead (II) Ions and Regeneration of the Exhausted Adsorbent. *Appl. Water Sci.* **2020**, *10*, 1–6. DOI: [10.1007/s13201-020-01250-y](https://doi.org/10.1007/s13201-020-01250-y).
- [85] WHO. **2017**. Guidelines for Drinking-Water Quality 4th Edition Incorporating the 1st Addendum. <https://www.who.int/publications/i/item/9789241549950> (accessed Jun 27, 2022).
- [86] Collivignarelli, M. C.; Canato, M.; Abbà, A.; Carnevale, M. M. Biosolids: What Are the Different Types of Reuse? *J. Clean Prod.* **2019**, *238*, 117–844.
- [87] Fuke, P.; T, M. M.; Kumar, M.; Sawarkar, A. D.; Pandey, A.; Singh, L. Role of Microbial Diversity to Influence the Growth and Environmental Remediation Capacity of Bamboo: A Review. *Ind. Crop Prod.* **2021**, *167*, 113567. DOI: [10.1016/j.indcrop.2021.113567](https://doi.org/10.1016/j.indcrop.2021.113567).
- [88] Kumar, V.; Singh, K.; Shah, M. P.; Kumar, M. Phytocapping: An Eco-Sustainable Green Technology for Environmental Pollution Control. *Bioremediation Environ. Sustain.* Elsevier, Amsterdam, Netherlands, **2021**, 481–491.
- [89] Ayawei, N.; Ebelegi, A. N.; Wankasi, D. Modelling and Interpretation of Adsorption Isotherms. *J. Chem.* **2017**, *2017*, 1–11. DOI: [10.1155/2017/3039817](https://doi.org/10.1155/2017/3039817).
- [90] Zhan, W.; Xinpei, D.; Hu, Z.; Xu, W.; Peng, S.; Khaliunaa, N.; Bushra, K.; Rooha, K. The Application of Error Function for Normalized Flux Prediction in Dead-End Microfiltration (MF) Process. *Sep. Sci Technol.* **2019**, *56*, 117–128.